Date July 27, 2018
Our reference n/a
Your reference n/a
Contact person S.P. Mulders
Telephone/fax +31 (0)6 5573 6149 / n/a
E-mail S.P.Mulders@TUDelft.nl
Subject Response to reviewers

Delft University of Technology

Delft Center for Systems and Control

Address
Mekelweg 2 (3ME building)
2628 CD Delft
The Netherlands

www.dcsc.tudelft.nl

Reviewers
Wind Energy Science

Dear Reviewers,

First of all, the authors would like to thank the reviewers for their positive and constructive feedback. We believe that the comments help us to significantly improve the quality of the paper. The objective of this document is to respond to the points raised by the reviewers (blue) and to provide an overview of the actions that are taken (red). When in this response the authors refer to adjustments in a particular section, figure or table, we ask the reviewer to refer to the marked-up manuscript version to evaluate the changes.

The document consists of five sections, each addressing the comments of the reviewers separately.

Yours sincerely,

Sebastiaan Paul Mulders
Niels Frederik Boudewijn Diepeveen
Jan-Willem van Wingerden

Enclosure(s): Response to comments of Reviewer 1
Response to comments of Reviewer 2
Response to comments of Reviewer 3
Response to comments of Reviewer 4
Response to comments of Reviewer 5

Response to comments of Anonymous Referee #1

Reviewer 1 comments: This paper presents an interesting analysis of a novel hydraulic wind turbine concept. The concept consists on replacing the conventional mechanical drivetrain components with a seawater pump directly driven by the wind turbine, whose outlet flow is directed to a Pelton generator. However, the analysis presented in the paper refers to an intermediate solution, in which the seawater pump is driven by a close loop oil-based hydrostatic transmission. The paper topic is certainly relevant for the journal; the approach is rigorous and the authors appear to be very familiar and qualified for work in the field. However, the paper could be significantly improved in certain aspects. Therefore, this Reviewer recommend its publication only after major changes are implemented to the submitted manuscript.

The authors thank the reviewer for his/her thorough review, invaluable comments and remarks. The considerations are especially informative as in particular considerations are raised on the analysis and justification of the hydraulic drivetrain and its components. Processing these comments very much helped the authors in closing the gap between system design and mathematical evaluation of the employed turbine with hydraulic transmission.

1. [Major] The paper is quite long, it contains too many equations and figures. This Reviewer suggests the authors to reduce the number of equations and figures. Some suggestions are provided in the following comments. Consider also that this Reviewers is asking for some additional details, therefore some additional figures might be necessary in the revised version of the paper.

   The authors agree with the fact that this paper is quite long. In the revised version, this issue is addressed by revising the relevance of all content. We are grateful of the reviewer suggestions, and the authors will take these remarks into account.

   The most notable changes are noted:
   - Section 2.2 is extended to provide a more detailed description of the DOT500 prototype set-up;
   - Section 3.2.1 is shortened, now only showing the results. The derivation is moved to the appendix;
   - Section 4.2.2 is shortened.

2. [Minor] Not sure about the significance of fig. 2, since the concept is quite obvious. In any case, if the authors decide to keep this image, this Reviewer suggests to include labels for the different components represented

   Thank you for this comment. The authors agree that this figure is not of direct scientific relevance, however, it presents a nice comparison of the (potential) space-advantage of a wind turbine with hydraulic drivetrain.

   The authors decided to keep the figure, but included a description of the distinct components, as suggested by the reviewer.

3. [Major] The authors provide a quite exhaustive overview of the past effort, which is very appreciated. However, at pag. 2, they affirm "To date, none of the above described full hydraulic concepts made its way to a commercial product. All concepts use oil as the hydraulic medium because of the favorable fluid properties and wide component availability, but therefore also need to operate in closed-loop." This Reviewer has two problems with such sentence:

   - For the size of the components required for wind turbine applications, there are almost no available commercial products. Those chosen by the authors in their work are probably the among the very few ones available (considering also that they had to turn a motor into a pump!). This is because as the authors stated, there are no successful application for hydraulic wind turbines. Therefore, if there is no market (thus no demand), there is no offer. The message is that nowadays someone wants to design a hydraulic wind turbine, he/she necessitates to design the hydraulic components as well (or partner with a component manufacturer to get a unit specially designed).

     The authors agree with the reviewer on this point. DOT is founded with the philosophy that offshore wind can be simplified and exploited more efficiently by centralizing energy production. However, to date, a water pump with capabilities to operate under high load and low speed is not commercially available. DOT is very aware of this, and is therefore (1) working to develop a seawater pump by their selves, and (2) actively cooperating with renowned (water) pump manufacturers on the development of such a pump.

     The in-field tests with an intermediate drivetrain including a closed oil circuit, is the first step towards the final DOT concept. The goal of DOT therefore is to abandon the use of oil all together by making wind turbines to cooperate and use what is abundantly available offshore: seawater. The authors (and DOT) do realize that a lot of hurdles need to be overcome before this goal becomes reality.

- The reference to close loop (close circuit ?) hydraulic transmissions (HTs) is questionable. HTs for many mobile applications (wheel loaders, excavators, etc) are close loop, but again the components for these HTs are too small for wind turbine applications. HTs can also be open-loop. Many HTs for areal platforms, forklifts, hydraulic fan drives are open-loop. What are the requirements that determine the need of having a close loop HT for a wind turbine application? This Reviewer can have some guesses, but this should be better addressed.

  The point raised by the reviewer is valid. A closed circuit drivetrain for a wind turbine utilizing oil as the hydraulic medium is needed because:
  (1) Operating a turbine with oil at remote offshore locations might pollute the environment in the event of a calamity;
  (2) Not having to provide a continuous fresh oil supply to the circuit;

  A consideration for operating in closed circuit is cooling of the hydraulic medium. When losses in hydraulic components are significant and the natural convection of heat to the surroundings is insufficient for cooling, an additional cooling circuit needs to be incorporated.

The authors recognize that the statement is posed too strong and lacks further explanation. Therefore, the comments of the reviewer and our considerations are processed in the revised version of the introduction. Furthermore, we made sure that we reserved the term "circuit" for hydraulic matters, and "loop" for control purposes.

4. [Minor] Was the concept of the paper presented also at the IFK2018 conference? A better reference to that paper, and the novel contents of this paper, should be provided.

   Yes, this is correct. We did not yet include a reference to the conference paper, as it was not published at time of submission of the WES manuscript.

   The authors included a reference to the conference article in the introduction, and stated clearly what the contribution of this paper is as opposed to the conference article.

5. [Minor] figure 3 might not be necessary, can be removed.

   Thank you for this comment. Because of the length and increased complexity of this paper we included a paper organization flow chart. However, providing both a textual and graphical outline might indeed be redundant.

   The figure is removed from the manuscript.

6. [Major] Section 2.2. The hydraulic circuit needs to be better detailed. A more realistic ISO schematic with respect to the one provided in fig. 6 is needed. The authors give the impression that a pump can be simply be coupled with a motor to form a close loop HT. However, other components are needed to guarantee the operation of the system:

   The authors agree with the reviewer that the hydraulic diagram should be better detailed. The included simplified hydraulic diagram was a trade-off between complexity and relevance for the drivetrain modeling provided in the manuscript. In the real-world set-up, numerous additional components were in place for turbine operation.

   Reconsidering the performed trade-off, the authors revisited the hydraulic diagram by including vital components. The components that are not included/considered for modeling and analysis are presented in gray. In this way, the authors think that the updated diagram provides a middle course from a system design and theoretical modeling point of view.

- Is a charge pump present? How was that sized? Can be neglected in the analysis? Why? What is the pressure level of the low pressure line? Is a flushing valve / cooling of the hydraulic motor present / necessary for the long operation of the system? A HTs for continuous operation usually necessitates for a significant oversizing of the charge unit for cooling purposes.

  Correct, charge pumps are presents in both the oil and water circuits. The oil charge pump was sized in such a way that a sufficient flow with a constant (controlled) feed-pressure of 21 bar to the oil pump could be delivered. Additionally when cooling was required, the charge pump supplied more flow to be directed through the parallel cooling circuit connected by a pressure relief valve (see updated hydraulic diagram). For the water circuit, the centrifugal charge pump provided a lower charge pressure of 2.6 bar. This difference in charge pressure is due to the different pump types used: the radial piston oil pump (motor) requires a higher charge pressure, as this is used to actively push the piston bearings to the cam ring; whereas the water plunger pump largely alleviates this requirement.

  As for modeling purposes of the closed oil circuit only pressure differences over the hydraulic components (taking into account mechanical/volumetric efficiency losses) are considered, the feed pressure is left out from the analysis. For the open water circuit however, the feed pressure is neglected because of its low value and for convenient derivation of the passive torque control strategy.

  Cooling equipment was indeed necessary for the closed oil circuit, and a flush oil cooling circuit was in place to ensure long-term operation and prevent the working fluid from overheating.

  The updated manuscript now provides a more detailed description of the aspects discussed above in Section 2.2.

- Circuit of the water pump. The authors say that there is an external centrifugal pump, which seems to be connected in series with the fixed displacement pump. How is the schematic? Is there a relief valve in between to provide a reference pressure level? Why this part can be neglected in the subsequent analysis?

  The reviewer is correct, the centrifugal pump is connected in series to the water pump, and the updated hydraulic diagram presents the working principle. To prevent a disturbed flow entering the water pump, a two-reservoir set-up is used. The speed of the centrifugal pump is controlled to maintain feed pressure of approximately 2.6 bars. The charge pump is enabled before the water pump starts speeding up to ensure feed-pressure and thus to avoid cavitation. The low-pressure side of the water circuit does not contain a pressure-relief valve, as the water plunger pump allows for a direct feed-though of the flow; the high-pressure side however does include a pressure relief valve.

  Section 2.2 is updated with the details provided in the response to the reviewer.

- Pelton Turbine. The concept of using a Pelton Turbine is very interesting. However, it seems that the Head [m] of this turbine is way above to the existing Pelton turbines, so that it might be impossible to borrow an existing design. What is the specific speed of the Pelton Turbine of this paper? Is a commercial Pelton wheel available? Is a two-jet turbine such as the one of fig. 5 sufficient? This is not the scope of this paper, however, the authors could be more clear on this part, perhaps using more references.

  Thank you for raising this comment, we could have been more clear on this aspect. Pelton turbines are highly specialized pieces of equipment and need to be design for specific condition requirements [1]. The Sy Sima 315 MW turbine in Norway, for 88.5 bar of head pressure is to date the largest known [2]. The employed custom manufactured Pelton turbine for the DOT500 is designed to match the nominal pressure and the speed conditions of the connected electrical generator.

  A custom-made Pelton turbine is designed such that the efficiency is optimal under the expected operational conditions. For this, the turbine is designed for optimal operation using 2 spear valves, subject to a nominal flow of 58 l/min. Graphs of the turbine manufacturer (given below) show that the efficiency is primarily a function of the supplied flow, and to a lesser extent of the head. The red line indicates operation with 1 spear valve, the blue line 2 spear valves.

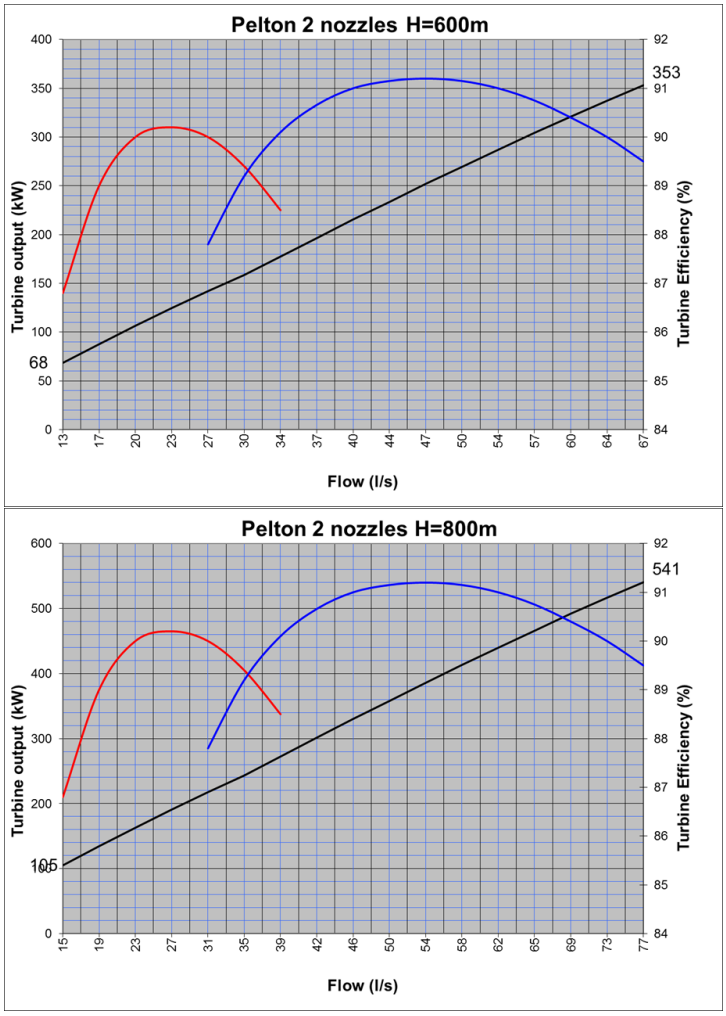

The efficiency aspect is confirmed later by experiments executed by DOT, of which an efficiency evaluation figure is also given below. In the figure an evaluation of the combined spear valve-Pelton efficiency from hydrostatic fluid to mechanical power at the generator axis is given as a function of flow and pressure. Whereas during the experiment the flow was not sufficient to explore the overall characteristics, the results clearly show that the steepest partial efficiency gradient goes with flow; at higher flow rates the gradient with respect to pressure becomes negligible.

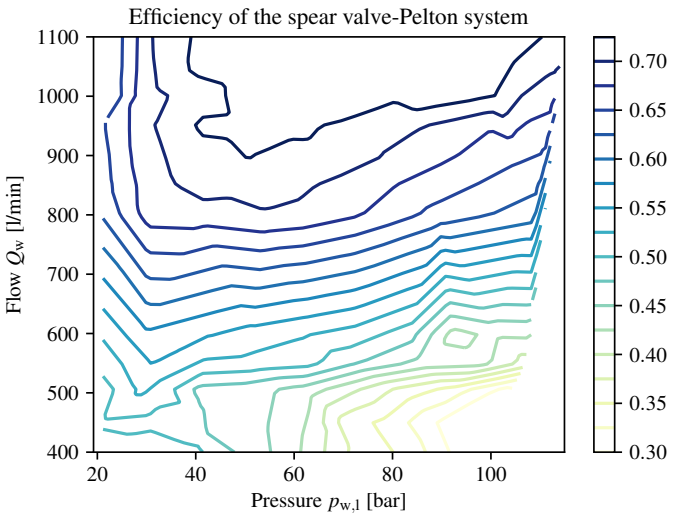

In the updated manuscript, more information on the custom-design Pelton turbine is given. Also the nominal operating conditions are discussed, and relevant references are included.

7. [Major] At page 7, the authors say After the water flow exits the spear valve, the aim to operate the Pelton turbine generator combination at maximum efficiency is a decoupled control objective from the rest of the drivetrain, and is outside the scope of this paper. Actually, this sentence is at the basis of many assumptions made in the development of the model and the controller design. This Reviewer, although without specific experience in designing HTs for wind turbine applications, has some conceptual doubts on this choice made by the authors. A HT has to be designed according to the features of both the load and the prime mover; this also drives several choices of constant torque (variable displacement pump) or constant power (variable displacement motor) HTs. In this case, the authors decide to neglect the features of the user (the Pelton wheel). Is that correct? To this Reviewer, it is like affirming that all the points that satisfies Eq. 12 (relation nozzle area and HT pressure) are indifferent for the Pelton turbine. This is quite hard to believe. The Pelton turbine should have preferred operating points that the HTs should be able to handle. This is a very basic question that the authors should address properly. Otherwise their proposed controller might not be beneficial on a real application.

   The reviewer correctly points out that the system design, as well as the applied control strategy should go hand-in-hand. Changing the operational strategy on the wind turbine side affects the operating point of the Pelton turbine and thereby for example the maximum amount of energy it can extract from the given flow. This is completely understood by the authors.

   The features of the Pelton wheel are not neglected. It is known from literature [3][4] that the ratio of tangential Pelton and water jet speed needs to be maintained at approximately $1/2$. As the Pelton wheel is mechanically coupled to an asynchronous generator, which can change its operational speed, a pressure measurement is used to determine the most favorable (speed) operating point to be as efficient as possible, given the conditions it is subjected to. However, the Pelton wheel will in the given set-up always be subjected to varying conditions, and thus suboptimal operation in the considered drivetrain using fixed-displacement components. This is for now a design choice, and further research needs to be conducted to elaborate on Pelton design and efficiency maximization given the varying operational conditions.

   The point of which operational path is most efficient, given varying Pelton conditions, remains. Operation at $C_{\tau,\max}$ will result in higher pressures for equal flows when compared to $C_{\mathrm{p,max}}$ operation. As was concluded in the previous question, the main driver determining the Pelton efficiency is the flow it is subjected to, whereas the head has negligible influence.

   The above given considerations are included in the manuscript in Section 2.2.

8. [Major] Section 3.1.2. The authors here affirm "the volumetric efficiency of a pump or motor is generally high and fairly constant over the entire operating range". For a simplified model the assumption of constant efficiency could be a fair starting point. But the statement that hydraulic pumps and motors have a constant volumetric efficiency for any pressure and shaft speed is clearly wrong. Otherwise, all the literature on empirical efficiency models (starting from Merritt in the 60s), standards for measuring volumetric efficiency (ISO, etc), tribological models for studying the lubricating gap flows, would not be justified. Particularly at low speed, the volumetric efficiency can be particularly low for both pumps and motors. Please revise this statement and better justify the assumption of constant efficiency, which can be very limited.

   The reviewer makes a very valid point, and we agree with it. The reason we have chosen to assume a constant volumetric efficiency factor is (1) the fact that for most of the given components, no volumetric efficiency data is available, and (2) the aim is to provide a simplified model of the hydraulic drivetrain.

   The assumption of a volumetric efficiency is revised in the updated manuscript.

9. [Minor] Section 3.2.1. here there are several equations that are well known. This section could be reduced.

   Thank you for this comment. The authors recognize that Section 3.2.1 is lengthy and reduced it. Now, only the major results are presented. However, we would like to be as complete as possible, seen the journal we are publishing in is not primarily focussed on hydraulics. Therefore, we moved the derivation of the results to the appendix.

   Section 3.2.1 is shortened and the derivation of the results has been moved to the appendix.

10. [Major] Section 3.2.2. In the list of assumptions it is stated that the inertia of the hydraulic components is neglected. While it is true that hydraulic components have fast dynamic, in comparison with other technologies for transmitting power, it has to be proven that within a hydraulic system the hydraulic line is the element with slowest dynamic. This statement, in general is not true, and Merritt never affirmed that. Moreover, the authors consider infinitely rigid lines, therefore the fastest lines possible (is this realistic?). Please justify this statement.

    Thank you for this comment, the authors agree with the reviewer that the (slow) line dynamics cannot be discarded. As exact specifications of the line bulk modulus are unknown (not publicly available), we decided to take a reasonable value of $K_\mathrm{l} = 0.8$ GPa from [5], which is twice as low as the bulk modulus value taken for the oil column. The equivalent bulk modulus is calculated by the relation $K_\mathrm{e} = (1/K_\mathrm{f} + 1/K_\mathrm{l})^{-1} = 0.52$ GPa. The equivalent value is used subsequently in the remainder of the paper.

    The assumption of infinitely rigid lines is removed from the analysis in Section 3.2.2, and Appendix A is updated to include relation for calculating the equivalent bulk modulus. The resulting equivalent modulus is subsequently used in the analyses throughout the different sections of the paper. Furthermore, Section 3.1.1 of the manuscript is updated, and now includes a more elaborate justification on why the drivetrain component dynamics are neglected and assumed as analytic expressions.

11. [Major] Section 4.1.1. The authors say "hydraulic components are known to be more efficient in high-load operating conditions, it might be advantageous for a hydraulic drivetrain to operate the rotor at a lower tip-speed ratio". This statement can be arguable. first, shaft speed has a major effect, and not all units have a clear trend with load. Can the authors provide the overall efficiency plot for the commercial units they utilize (even in normalized form?). This is very important, because all the controllers of case 1 and case 2 are based on this assumption!

    The authors agree with the comment made by the reviewer, and the statement the reviewer refers to is changed. However, the manuscript already includes (mechanical) efficiency data for the oil pump and motor, given in Figure 13. The figure includes the proposed operational strategies (case 1 and case 2), and a steady-state analysis of the total drivetrain efficiency for both strategies is given in Figure 14.

    The titles of the plots in Figure 13 and the legend in Figure 14 are now updated, to make their purpose more clear. Also, the statement the reviewer refers to is adjusted, and an additional consideration on the efficiency aspect is made in Section 4.1.2.

12. [Minor] Pag. 21. The reference to fig 14 might be wrong, since the figure refers to mechanical efficiency.

    Thanks for pointing out this mistake. The reference should be pointing to Fig. 13.

    The reference is corrected in the revised manuscript.

13. [Major] 4.2.1. L=50m... are the pump and motor connected by a 50 m straight line? If there are line discontinuities, some terms, particularly the inductance terms, can be entirely wrong

    Indeed, apart from a swivel which enables continuous yaw motion located below the nacelle, the high pressure lines have no discontinuities, and run from the nacelle all the way to the oil motor located in the monopile. Furthermore, the rotor inertia, which is expressed in terms of hydraulic induction, is predominant in the lumped induction term. The contribution of the hydraulic inductance term is thus negligible, and discrepancies would have a negligible effect on the analysis.

Response to comments of Anonymous Referee #2

Reviewer 2 comments: Thank you for your submission. In general I found the paper to be interesting and well-presented. Background literature was complete and informative, and the introductory material explains well what this paper adds to the growing literature. The figures and illustrations are particularly well done and helpful. The writing is clear, with only very few grammatical errors. The paper is well structured, such that one new to hydraulic drivetrain wind can follow. Finally, the inclusion of field results and comparing to the theoretical work is informative. Excellent work.

Thank you, the authors are pleased to read this!

Therefore, only a few comments to be given, overall:

1. Is there provided, or could the authors provide, a quick impression of how the efficiency of the proposed system, in total, would compare to a similar conventional system? For example, given the same rotors, what would a standard efficiency to final electrical power be (90%?) and what would it be for this system?

   For the described DOT prototype, the total power transmission efficiency was predictably low, as a result of the double hydraulic circuit. In the below-rated region an efficiency is attained of $30-45\,\%$ depending on the operating conditions, whereas in the above-rated region a consistent drivetrain efficiency of $45\,\%$ is attained. As described in the manuscript, off-the-shelf components are used, of which the optimal efficiency operational envelopes do not match. The drivetrain has a fixed-volumetric displacement, which means that the pressure and flow changes according to the turbine operating conditions. Figure 13 shows that drivetrain components have a specific region in which they yield maximum efficiency.

   The above given reasoning holds for the described prototype. It is however yet unclear what the drivetrain efficiency of the final DOT concept will be, as the seawater pump is still under development. An earlier PhD thesis on hydraulic wind turbine networks [7] provides an estimate on the overall conversion efficiency of conventional and hydraulic wind turbines of $82-84\,\%$ and $70-80\,\%$, respectively.

   The efficiency numbers attained with the intermediate DOT500 prototype are added to Section 2.1.

   Specific:

2. 3.2.1: "and vice versa for the latter.." I could not fully understand what is meant by this. Could a Bode plot of the transfer functions be included to visualize the inverted notch functions?

   The authors did separate the theory from the results. For this reason, in Section 3.2.1, only theory is provided, whereas in Section 4.2.1 an illustrative example is given, which considers the system and hydraulic properties of the DOT500 system. In the latter mentioned section, a Bode plot of the of the transfer function $G_{\mathrm{Q}/\Delta\mathrm{p}}(s)$ is given. For clarity reasons (and considering the length of the paper), a visualization of $G_{\Delta\mathrm{p}/\mathrm{Q}}(s)$ is omitted in the manuscript, but given in the figure below. It is shown that the inverted notch characteristics is still present. However, exciting the flow (instead of pressure) results in amplification/transmission to pressure in a wider frequency region for shorter line lengths. For longer line lengths, the amplification magnitude increases, but at a more specific interval. This effect is a result of the inverse proportionality between the damping coefficients ζ_{Q} and ζ_{p}.

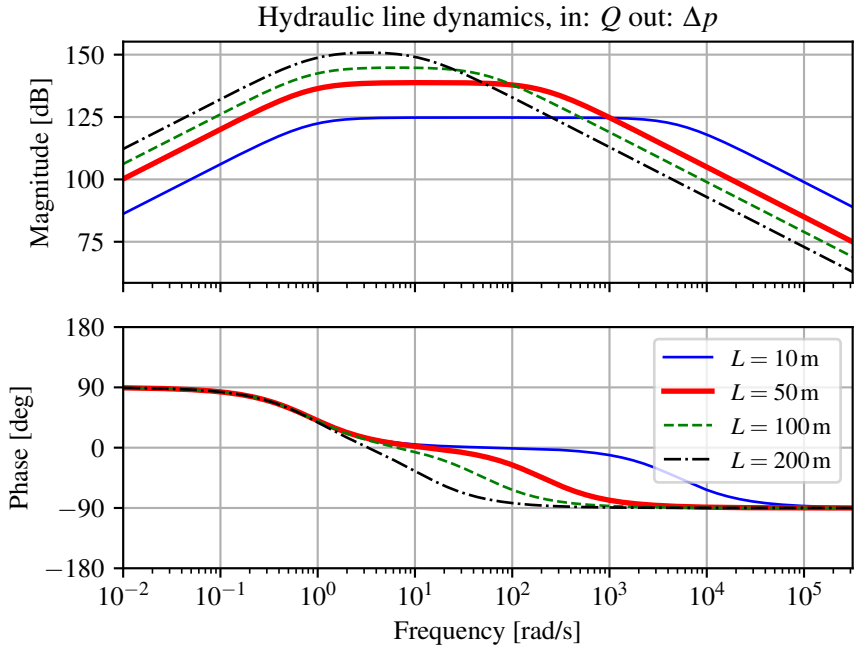

In Section 3.2.1 the phrase "and vice versa for the latter.." is removed and replaced with a more convenient description. The paragraph now also references to the illustrative example in Figure 15.

3. Eq 38: The B-matrix in this version includes the inputs? There is a dot following the matrix but it is not clear what the dot product will be with? In eq 54 there are only 3 columns total for the 3 B matrices, but are there 4 variables provided in this version?

   The representation given by Eq. 38 is the rewritten form of the dynamic system derived in in Eqs. (33)-(37). There is no dot-product after the input vector, this is just punctuation to indicate the end of the sentence. The pressures Δp_{h} and Δp_{b} cannot be controlled directly. For this reason, the rotor torque and spear valve pressure characteristics are evaluated and linearized at different operating points. By doing so, a linear state space system defined in Eq. (54) is obtained. By substitution of the linearized characteristics, defined in Eqs. (46) and (51), the terms redistribute in the A, B and B_{U} matrices: some are defined in the state vectors, others can be regarded as control inputs or wind disturbance inputs in B and B_{U}.

   The authors hope to have clarified the unclarities, and slightly updated the section to improve readability.

4. Section 4.1.1: "advantageous for ... operate a lower tip-speed ratio", this is counterintuitive, but do I understand correct that although the rotor power will be reduced, the improved hydraulic efficiency will lead to higher final electrical power? Is this demonstrated conclusively?

   The reviewer is correct. Normal wind turbines operate the rotor at the maximum power coefficient, maximizing the efficiency in the below-rated region. For the DOT500, however, the wind turbine drivetrain is retrofitted, while retaining the original turbine rotor. As hydraulic components are in general more efficient in high-load operating conditions, we additionally perform an analysis for operating the turbine at the maximum possible torque coefficient. The maximum torque coefficient is located at a lower tip-speed ratio (lower rotor speeds, higher torques for equal wind speeds), and corresponds with a lower power coefficient.

   So indeed, from a aerodynamic efficiency perspective this is unfavorable, but from a hydraulic drivetrain perspective this might result in an overall efficiency advantage. In the subsequent section, an efficiency analysis is given on a component level for both operating cases in Figure 13, and an overall evaluation of the drivetrain efficiency is presented by Figure 14. The analysis takes into account the reduced rotor power coefficient for operation at maximum torque.

   The titles of the plots in Figure 13 and the legend in Figure 14 are now updated, to make their purpose more clear. Also the introductory paragraph of Section 4.1.1 is updated, and a concluding remark referring to the next section where the actual efficiency analysis is performed is added.

5. Section 4.1.2: Does the lower TSR also risk increased occurrence of dynamic stall?

   Thank you, this is a very good question. We cite the following phrase from [8]:

   "Stall on lifting surfaces is commonly encountered, mostly undesired, and occurs when a critical angle of attack is exceeded. Depending on the unsteady rate of change of the airfoil's angle of attack, static and dynamic stall are distinguished. (...) During dynamic stall, the shear layer rolls up into a large scale dynamic stall vortex which grows locally and temporally until vortex induced separation occurs. During static stall on the other hand, the shear layer rolls up continuously into large-scale structures that grow spatially."

   So indeed, there is an increased occurrence of dynamic stall, especially in turbulent wind conditions when the angle of attack continuously varies.

   Furthermore, from a discussion with a professor in aerodynamics from our faculty, it became clear that (dynamic) stall could indeed occur in the region of the blade root. Stalling of a larger blade would result in increased loading with a reduced power capture, however, as we are not stalling during normal operation, the effects on loads should be minor. He also clarified that dynamic stalling could even be slightly beneficial, as it introduces a dissipating/damping effect.

   We have to admit that we did not perform a detailed analysis on this aspect. The aim of the in-field test was to show the feasibility of the hydraulic drivetrain, and while we ensured safe operation of the turbine, effects such as dynamic stall were disregarded. The authors have noted the comment, and the effects of (dynamic) stall will be considered in later stages of the project.

6. Fig 16: Title is incomplete

   Correct, thank you for pointing out. We referred back to the submitted manuscript, but there the title is correct. Somehow, processing of the manuscript during upload must have changed the title by accident.

7. Fig 18: The legend is hard to understand, why the lower-case bold "without" following the period? Since the phase margin is discussed later, could it be indicated in this figure?

   Thank you for pointing out this mistake, the point should be a comma. The suggestion of indicating the phase margin is taken, and both bode plots are updated.

Also, again, the upload process changed the figure, by omitting some symbols. The correct figure is shown below for reference.

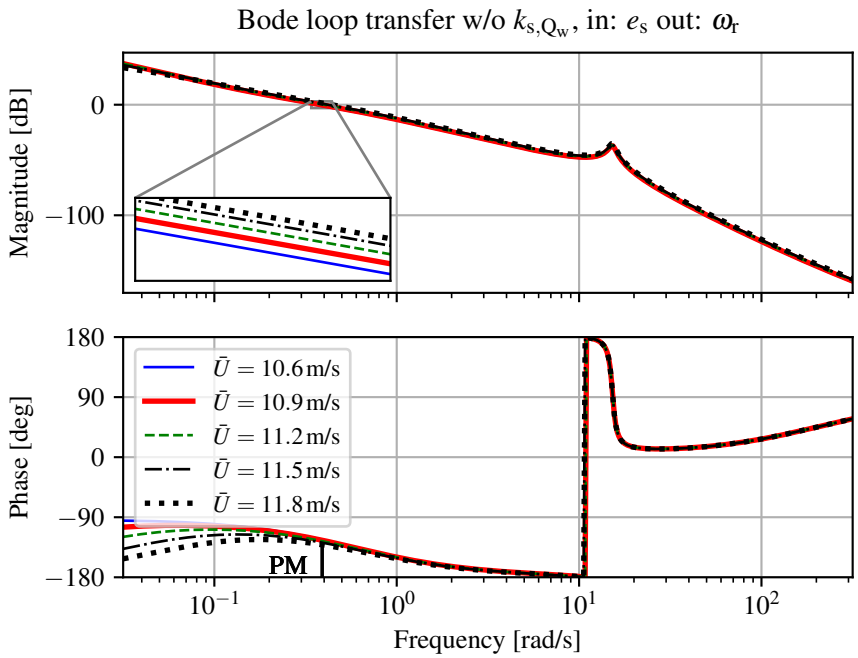

The mistake in the caption is fixed, and the Bode plots include an indication of the phase margin (PM).

8. Fig 22: Color legend missing label

The point raised by the reviewer is not entirely clear for the authors. Figure 21 is a representation of the tip-speed ratio for a range of turbine operating points. This is also stated title and the caption of the figure. Adding an additional label to the color legend would be redundant in our opinion.

9. Fig 24: Good figure, just wish to confirm, is rotor speed scaled correctly? Does it always stay so close to its maximum? Or is this period special in that there is only a brief excursion into region 2 (which makes sense, youve selected a period covering 2,2.5,3) just want to be sure.

   Thank you for this comment. Yes, the rotor speed is scaled correctly, however, we took a part of the time-series where the environmental conditions were such that the turbine operated around region 2.5. What we want to show in this figure is how the spear valve torque controller (only active in region 2.5) works as expected and switches nicely to region 2 (no control), and region 3 (pitch control).

   The text is adjusted slightly such that the purpose of the figure is more clear.

   An interesting, and well-presented paper.

   Thanks again!

Response to comments of Anonymous Referee #3

Paper is very well written and subject matter thoroughly presented.

Thank you, the authors are grateful to hear this.

Some general comments: towards the beginning of the paper it is stated that "To date, none of the above described full hydraulic concepts made its way to a commercial product", this merits some justification as to why the concept of hydraulic transmission for wind turbines has not been commercially viable so far, and whether the presented work can potentially overcome these barriers to market.

The authors agree with the reviewer, and a similar points has been posed by Referee #1. We would like to refer the reviewer to the answer given in Question 3-2 in our response to the first referee.

We further elaborated on this point in the introduction of the manuscript according to the comments of both referees.

One minor comment would be to add some labelling of the components in figure 2.

Thank you for this comment. We agree that labelling of the components improves the quality and relevance of the figure.

The figure is updated accordingly, now including labels indicating the components.

Response to comments of Anonymous Referee #4

The research in the paper is original, well conceived, and of interest to the readers of this journal. The other reviewers have done a good job in providing a detailed review.

Thank you, we are grateful to read this positive comment.

I only have one comment. The reviews advocate maximizing the torque coefficient rather than maximizing the power coefficient for this particular case. They further demonstrate that this provide more energy for the system considered since hydraulic components in this particular case are more efficient at higher torque and lower speed.

It is important to point out that while the torque coefficient optimizing approach is advantageous in this particular case, it is not true in general. The overall efficiency of a hydraulic pump or motor is the product of the mechanical efficiency and the volumetric efficiency. Depending on the particulars of the unit and its operating conditions, either of these might be dominant. A truly rigorous approach would be to optimize the system power coefficient with all losses included. This would work for any case.

In their final version the authors must clearly state that the torque coefficient optimization approach they advocate is true in this case, but is not true in general.

The authors completely agree with the referee. Only two cases are considered in this paper, namely: operation at rotor maximum torque, and maximum power coefficient. For the specific case presented in the paper, it is found that the maximum torque case results in the highest overall drivetrain efficiency. However, this claim can by no means be generalized for other wind turbines with hydraulic drivetrains. A more rigorous approach would indeed be to optimize the ideal below-rated operational trajectory subject to all component characteristics. However, to perform a more concise analysis, only the two given trajectories are evaluated. For other set-ups it could indeed be the case that a different below-rated operating strategy is beneficial.

The consideration of the reviewer and our response is processed and included in Section 4.1.2.

Response to comments of Anonymous Referee #5

This is an interesting paper that deals with the use of hydraulic transmission systems to enable centralized conversion of wind power into electricity in offshore wind farms. A key advantage of this approach is the significant reduction in the nacelle weight. The paper is relevant and very timely given the present drive by industry to develop larger and heavier rotors. The following is a summary of the main comments that need to be addressed by the authors before the paper may be published:

The authors thank the reviewer for his positive comment and considerations raised.

1. Figure 5 may be deleted without affecting the quality of the paper.

   Indeed, the figure could be deleted. However, seen the journal we are publishing in is not primarily focussed on hydraulics, we think that the figure is insightful and serves readers from various disciplines.

   The authors would like to leave the figure as-is in the manuscript.

2. Table 1: It is also convenient for the reader to include the rated power of the motors

   Thank you for this comment, this is indeed a nice addition.

   Table 1 now includes the available power range of all the drivetrain components.

3. Page 6: The process of matching the pump, motor and Pelton turbine to the available wind turbine should be elaborated in further detail.

   Thank you for this comment. A description of the component matching process is not provided in detail in this paper, as the aim of the authors in this paper is to focus on the modeling and control design of the considered hydraulic drivetrain. One of the authors devoted his PhD to the system design of the presented drivetrain [9], and the authors refer the reviewer to this work for further details.

   The reference to the PhD thesis, including an elaborate description of the component matching process, is now also included in Section 2.2.

4. Page 9: specify the aerofoil data used in plotting Fig. 7.

   The presented power and torque coefficient curves are obtained from a Bladed wind turbine model which was shared confidentially with DOT. The model includes the requested airfoil data, but for reasons of confidentiality, this information cannot be shared publicly. However, the complete data set including the resulting power, torque and thrust coefficient tables (as a function of tip-speed ratio and blade pitch) is publicly available as an external asset [10].

   Section 3.1.1 now includes a reference to the externally available data set which includes power, torque and thrust coefficient tables.

5. Fig. 14: for ease of comparison, the two plots should have the same colour scale for the mechanical efficiency.

   We partly agree with the reviewer's remark. The color scales of the left and right plots range from 0.7 - 1.0 and 0.05 - 1.0, respectively. For plots with equal data (efficiency) ranges, we agree with the reviewer that equalizing them would enhance the readability. However, by using the same color bars for the presented plots would make the left plot less convenient to read by a lack of contrast (especially in grayscale). For this reason, the authors decided to leave the plots unchanged.

6. Figure 15: Possible design amendments to the system to enhance the overall conversion efficiency should be elaborated in further detail.

   A similar point is posed by reviewer #4, but focuses on the control aspect, and the authors refer the reviewer to our response in the previous section. In summary: for the considered system, only two scenarios are evaluated (maximum rotor power and maximum rotor torque trajectories) to provide a concise evaluation of both strategies on the overall drivetrain efficiency. Indeed, a more rigorous approach would be to optimize the ideal below-rated operational trajectory subject to all component characteristics.

   From a system design perspective, the presented prototype hydraulic wind turbine has the goal of showing the feasibility of a wind turbine with a hydraulic drivetrain, and is not meant to be kept as-is. In response to the first question of reviewer #2, we added the efficiency numbers of the current set-up to Section 2.1 ($30 - 45$ % below-rated, 45 % above-rated). Also, in Section 2.1, it is stated that the set-up allows for prototyping, and provides a proof of concept for faster development towards the ideal DOT concept. It is known that the additional components and energy conversions result in a reduced overall efficiency. For an overall increased efficiency, the amount of energy conversion steps need to be reduced. It is stated in the conclusion that by discarding the oil loop in the ideal DOT concept, only including a single water pump in the nacelle, the control design process is simplified and the overall drivetrain efficiency should be greatly improved.

   Regarding the changes already made to the manuscript, the authors think that the point raised by the reviewer is clarified.

Minor comments:

1. Figure 1 should ideally be presented on the same page where it is being referred to in the text.
2. Page 6, line 13 - remove coma after in such a way.
3. Eqt. (11) may be deleted as derived of Eqt (12) is well known.
4. Page 12, line 9 - remove coma after into the system.

Thank you for pointing out these minor remarks.

1. We agree with the reviewer, however, during typesetting the paper will be converted to a two-column format, and thus the complete mark-up will be changed again. We tried to make the figure positions as convenient as possible, but we are reticent on putting too much effort in this for now. However, we certainly keep this comment in mind for all figures during the mark-up of the final version of the manuscript.
2. Thank you, we corrected this.
3. We agree with the reviewer and deleted the equation.
4. Thank you, we corrected this.

References

[1] H. Brekke, *Hydraulic turbines: design, erection and operation*. Norwegian University of Science and Technology (NTNU), 2001.

[2] E. Cabrera, V. Espert, and F. Martínez, *Hydraulic Machinery and Cavitation: Proceedings of the XVIII IAHR Symposium on Hydraulic Machinery and Cavitation*. Springer, 2015.

[3] Z. Zhang, "Flow interactions in pelton turbines and the hydraulic efficiency of the turbine system," *Proceedings of the Institution of Mechanical Engineers, Part A: Journal of Power and Energy*, vol. 221, no. 3, pp. 343–355, 2007.

[4] J. Thake, *The Micro-hydro Pelton Turbine Manual*. Rugby, Warwickshire, United Kingdom: Practical Action Publishing, 2000.

[5] L. Hružík, M. Vašina, and A. Bureček, "Evaluation of bulk modulus of oil system with hydraulic line," in *EPJ Web of Conferences*, vol. 45. EDP Sciences, 2013, p. 01041.

[6] Bosch-Rexroth, "Axial piston variable motor a6vm - sales information/data sheet," Bosch-Rexroth, Tech. Rep., June 2012.

[7] A. Jarquin Laguna, "Centralized electricity generation in offshore wind farms using hydraulic networks," Ph.D. dissertation, Delft University of Technology, 2017.

[8] K. Mulleners and M. Raffel, "Static versus dynamic stall development," in *APS Meeting Abstracts*, Nov. 2012, p. L24.008.

[9] N. Diepeveen, "On the application of fluid power transmission in offshore wind turbines," Ph.D. dissertation, Delft University of Technology, 2013.

[10] S. P. Mulders, N. F. B. Diepeveen, and J.-W. van Wingerden, "Data set: Control design, implementation and evaluation for an in-field 500 kW wind turbine with a fixed-displacement hydraulic drivetrain," May 2018. [Online]. Available: https://doi.org/10.5281/zenodo.1250459

Control design, implementation and evaluation for an in-field 500 kW wind turbine with a fixed-displacement hydraulic drivetrain

Sebastiaan Paul Mulders[1], Niels Frederik Boudewijn Diepeveen[2], and Jan-Willem van Wingerden[1]

[1]Delft Center for Systems and Control, Faculty of Mechanical Engineering, Delft University of Technology, Mekelweg 2, 2628 CD Delft, The Netherlands

[2]DOT B.V., Raam 180, 2611 WP Delft, The Netherlands

Correspondence: Sebastiaan Paul Mulders (s.p.mulders@tudelft.nl)

Abstract. The business case for compact hydraulic wind turbine drivetrains is becoming ever stronger, as offshore wind turbines are getting larger in terms of size and power output. Hydraulic transmissions are generally employed in high load systems, and form an opportunity for application in multi-megawatt turbines. The Delft Offshore Turbine (DOT) is a hydraulic wind turbine concept replacing conventional drivetrain components with a single seawater pump. Pressurized seawater is directed to a combined Pelton-generator combination on a central multi-megawatt electricity generation platform. This paper presents the control design, implementation and evaluation for an intermediate version of the ideal DOT concept: an in-field ~~500~~500 kW hydraulic wind turbine. It is shown that the overall drivetrain efficiency and controllability is increased by operating the rotor at maximum rotor torque in the below-rated region using a passive torque control strategy. An active valve control scheme is employed and evaluated in near-rated conditions.

1 Introduction

The drivetrain of horizontal-axis wind turbines (HAWTs) generally consists of a rotor-gearbox-generator configuration in the nacelle, which enables each wind turbine to produce and deliver electrical energy independent of other wind turbines. While the HAWT is a proven concept, the turbine rotation speed decreases asymptotically and torque increases exponentially with increasing blade length and power ratings (Burton et al., 2011). As offshore wind turbines are getting ever larger, this results in a lower rotation speed and higher torque at the rotor axis. This inevitably leads to design challenges when scaling up conventional turbine drivetrains for the high-load subsystems (Kotzalas and Doll, 2010). The increased loads primarily affect high-weight components in the turbine such as the generator, bearings and gearbox, and makes repair and replacement a costly and challenging task (Spinato et al., 2009; Ragheb and Ragheb, 2010). Furthermore, due to the contribution of all nacelle components to the total nacelle mass, the complete wind turbine support structure and foundation is designed to carry this weight for the entire expected lifetime, which in turn leads to extra material, weight and thus total cost of the wind turbine (EWEA, 2009; Fingersh et al., 2006).

In an effort to reduce turbine weight, maintenance requirements, complexity, and thus the Levelized Cost Of Energy (LCOE) for offshore wind, hydraulic drivetrain concepts have been considered in the past (Piña Rodriguez, 2012). Integration of hydraulic transmission systems in offshore wind turbines seems to be an interesting opportunity, as they are generally employed

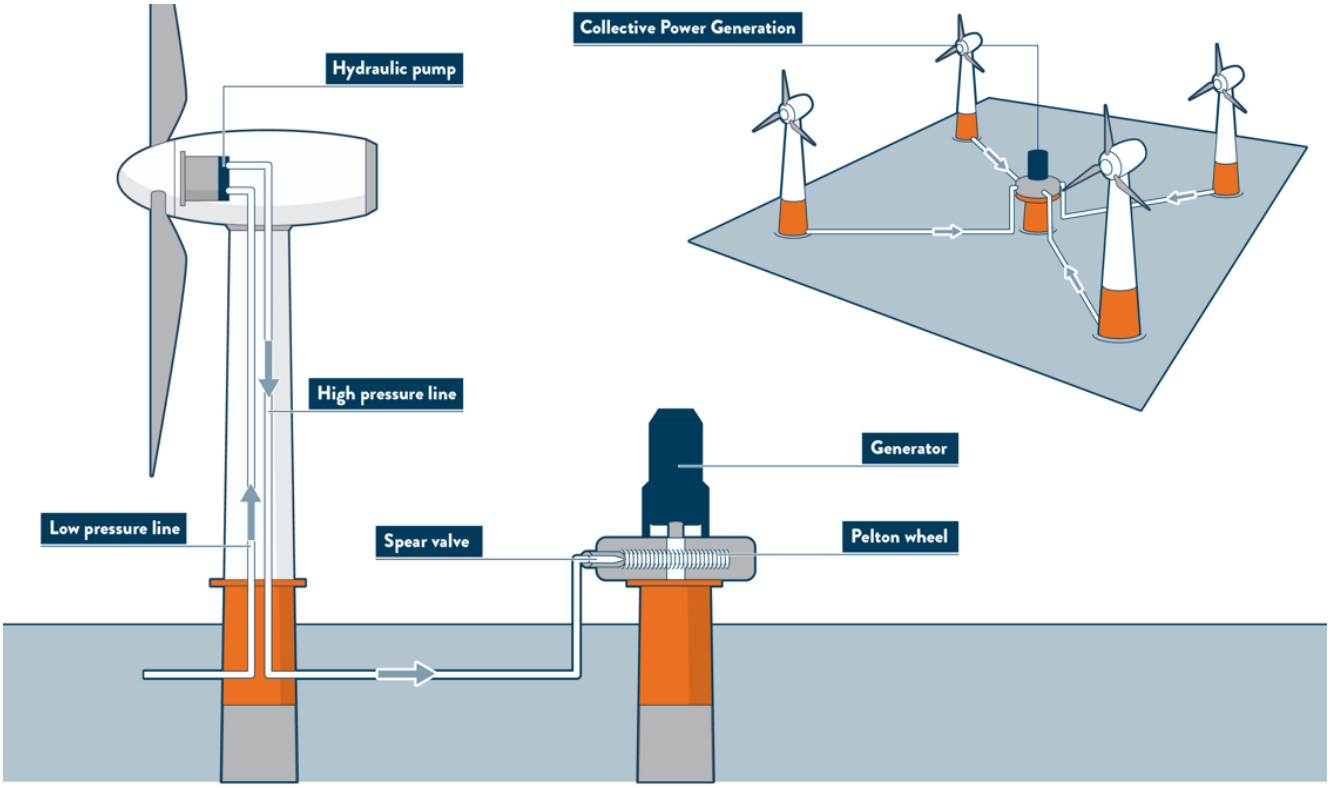

Figure 1. Schematic overview of an ideal DOT hydraulic wind turbine configuration. A radial piston seawater pump is coupled to the rotor in the nacelle. The flow is converted to a high-velocity water jet by a spear valve, and a Pelton turbine-generator configuration harvests the hydraulic into electric energy. Multiple turbines can be connected to the central power generation platform.

in high-load applications and have the advantage of a high power-to-weight ratio (Merritt, 1967). It is concluded in (Silva et al., 2014) that hydrostatic transmissions could lower drivetrain costs, improve system reliability and reduce the nacelle mass.

Various hydraulic turbine concepts have been considered in the past. The first ~~3~~3 MW wind turbine with a hydrostatic power transmission was the SWT3, developed and build from 1976 to 1980 by Bendix (Rybak, 1981). After deployment of the turbine with fourteen fixed-displacement oil pumps in the nacelle and eighteen variable-displacement motors at the tower base, it proved to be overly complex, inefficient and unreliable. With the aim to eliminate the power electronics entirely by application of a synchronous generator, Voith introduced the WinDrive in 2003 and provides a hydraulic gearbox with variable transmission ratio (Muller et al., 2006). In 2004, the ChapDrive hydraulic drivetrain solution was developed with the aim to drive a synchronous generator by a fixed-displacement oil pump and variable displacement oil motor (Chapple et al., 2011; Thomsen et al., 2012). Although the company acquired funding from Statoil for a ~~5~~5 MW concept, the company ceased operations. In cooperation with Hägglunds, Statoil modelled a drivetrain with hydrostatic transmission, consisting of a single oil pump connected to the rotor and six motors at ground level (Skaare et al., 2011, 2013). Each motor can be enabled or disabled to obtain a discrete variable transmission ratio to drive a synchronous generator. In 2005, Artemis Ltd. developed a

Figure 2. The high power-to-weight ratio of hydraulic components and the possibility to abandon power electronics from the nacelle, make the advantages of mass and space reductions in the nacelle self-evident.

digital displacement pump, meaning that it can continuously adjust its volume displacement in a *digital* way by enabling and disabling individual cylinders (Rampen et al., 2006; Artemis Intelligent Power, 2018). In 2010, Mitsubishi acquired Artemis Intelligent Power and started testing of its SeaAngel ~~7~~7 MW turbine with hydraulic power drive technology in 2014 (Sasaki et al., 2014).

~~To~~ The above described full hydraulic concepts aim to eliminate power electronics from the turbine for use of a synchronous generator, and therefore use a mechanism to vary the hydraulic gear ratio. However, to date, none of the ~~above described full hydraulic~~ concepts made its way to a commercial product. All concepts use oil as the hydraulic medium because of the favorable fluid properties and ~~wide~~ component availability, but therefore also need to operate in ~~closed-loop. The concepts aim to eliminate power electronics from the turbine for use of a synchronous generator, and therefore need a mechanism to vary the hydraulic gear ratio.~~ closed circuit. Closed circuit operation for an offshore wind application using oil is required to minimize the risk of environmental pollution, but also to abandon the need for a continuous fresh oil supply to the circuit. Furthermore, often an additional cooling circuit is needed when losses in hydraulic components are significant and natural heat convection to the surroundings is insufficient.

A novel and patented hydraulic concept with an ~~open-loop~~ open circuit drivetrain using seawater as the hydraulic medium is the Delft Offshore Turbine (DOT) (Van der Tempel, 2009)~~. This concept~~ , and is shown in Figure 1~~,~~. The open circuit is enabled by the use of preconditioned seawater, and alleviates the need for a cooling circuit by the continuous fresh supply. The DOT concept only requires a single seawater pump directly connected to the turbine rotor. The pump replaces components with high-maintenance requirements in the nacelle, which reduces the weight, support structure requirements and turbine maintenance frequency. This effect is clearly visualized in Figure 2. All maintenance critical components are located at sea level, and the centralized generator is coupled to a Pelton turbine. Turbines collectively drive the Pelton turbine to harvest the hydraulic into electrical energy. A feasibility study and modeling of a hydraulic wind turbine based on the DOT concept is performed in (Diepeveen, 2013). Hydraulic wind turbine networks employing variable displacement components are modeled and simulated in (Jarquin Laguna, 2017). Besides, using the DOT concept, a wind turbine drivetrain to generate electricity and simultaneously extract thermal energy has been proposed in (Buhagiar and Sant, 2014).

This paper presents the first steps in realizing the integrated hydraulic wind turbine concept, by full-scale prototype tests with a retrofitted Vestas V44 ~~600~~600 kW wind turbine, of which the conventional drivetrain is replaced by a ~~500~~500 kW hydraulic configuration. A spear valve is used to control the nozzle outlet area, which in effect influences the fluid pressure in the hydraulic discharge line of the water pump, and forms an alternative way of controlling the reaction torque to the rotor. Preliminary results of the in-field tests are presented earlier in (Mulders et al., 2018a).

The main contribution of this paper is to elaborate on mathematical modeling and controller design for a hydraulic drivetrain with fixed-displacement components, subject to efficiency and controllability maximization of the system. The control design is based on steady-state and dynamic turbine models, ~~and is~~ which are subsequently evaluated on the actual in-field retrofitted ~~500~~500 kW wind turbine. ~~Paper organization flow diagram.~~ Furthermore, a framework for modeling of fluid dynamics is provided, a parameter study on how different design variables influence the controllability is given and future improvements on the system and control design are proposed.

The organization of this paper is ~~visualized in Figure ??~~as follows. In Sect. 2, the DOT configuration used during the in-field tests is explained, and drivetrain components are specified. Section 3, which involves drivetrain modeling, is divided into two parts: a steady-state drivetrain model is derived in Sect. 3.1, and a drivetrain model including fluid dynamics is presented in Sect. 3.2. Controller design is performed in Sect. 4, where the steady-state model is used in Sect. 4.1 for the design of a passive control strategy for below-rated operation, whereas in Sect. 4.2 the dynamic model is used to derive an active control strategy for the region between below- and above-rated operation (near-rated region). Because the in-field tests are performed prior to theoretical model derivation and control design, preliminary conclusions from these tests are incorporated. In Sect. 5, in-field test results are presented for evaluation of the overall control design. Finally, in Sect. 6, conclusions are drawn and an outlook of the DOT concept is given.

2 The DOT500 - prototype turbine with off-the-shelf components

In this section, the intermediate prototype DOT turbine on which in-field tests are performed is described in Sect. 2.1. Subsequently, the drivetrain components used for the intermediate concept are discussed in Sect. 2.2.

2.1 The intermediate DOT500 prototype

At the time of writing, a low-speed high-torque seawater pump required for the ideal DOT concept is not commercially available. This pump is being developed by DOT, enabling the ideal concept in later stages of the project (Nijssen et al., 2018). An intermediate set-up using off-the-shelf components is proposed to speed up development and test the practical feasibility. A visualization of the DOT500 set-up is given in Figure 3.

A Vestas V44 ~~600~~600 kW turbine is used and its drivetrain is retrofitted into a ~~500~~500 kW hydraulic configuration. The original Vestas V44 turbine is equipped with a conventional drivetrain consisting of the main bearing, a gearbox and a ~~600~~600 kW three-phase asynchronous generator. The blades are pitched collectively by means of a hydraulic cylinder, driven by a HPU (Hydraulic Power Unit) with a safety pressure accumulator. The drivetrain of the Vestas turbine is replaced by a hydraulic

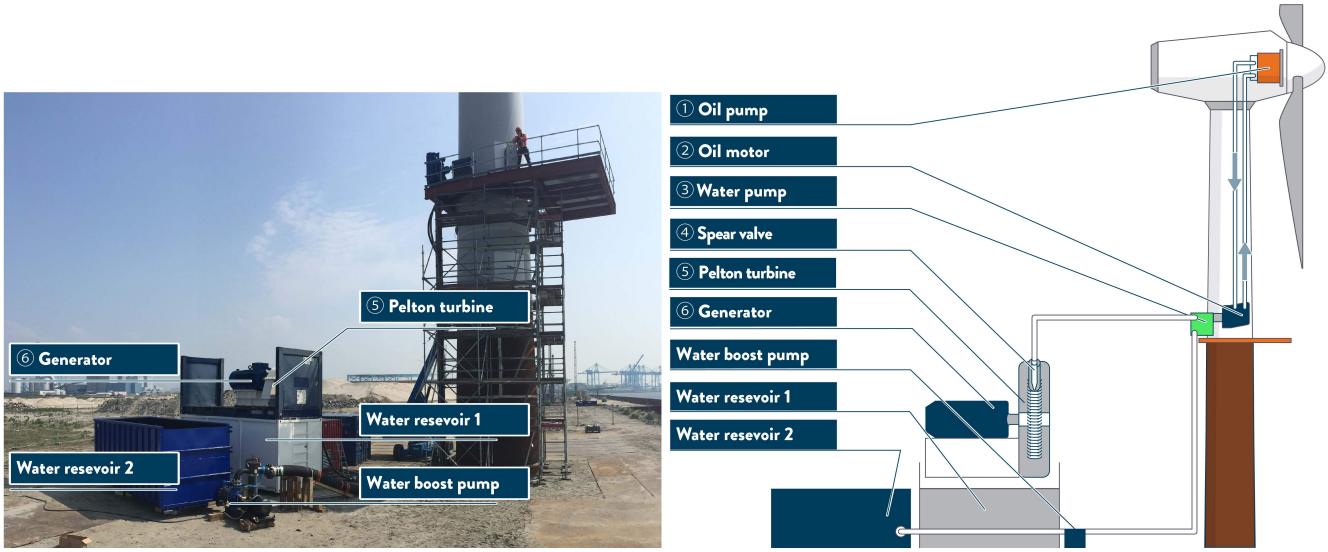

Figure 3. Overview of the intermediate DOT500 hydraulic wind turbine configuration. An oil pump is coupled to the rotor low-speed shaft in the nacelle and hydraulically drives an oil motor in the bottom of the tower. This closed oil circuit serves as a hydraulic gearbox between the rotor and water pump. The motor is mechanically coupled to a water pump which produces a pressurized water flow. The flow is converted to high-velocity water jets by spear valves and a Pelton turbine-generator configuration harvests the hydraulic into electric energy.

drivetrain. This means that the gearbox and generator are removed from the nacelle, and replaced by a single oil pump coupled to the rotor via the main-bearing.

In the retrofitted hydraulic configuration, a low-speed oil pump is coupled to the rotor and its flow hydraulically drives a high-speed oil motor-water pump combination at the bottom of the turbine tower. The oil circuit acts as a hydraulic gearbox between the rotor and the water pump. The water circuit including Pelton-generator combination is as in the ideal set-up depicted in Figure 1. It is known and taken into account that the additional components and energy conversions result in a reduced overall efficiency: the in-field tests show a below-rated efficiency in the range of 30 – 45 %, whereas in the above-rated region a drivetrain efficiency of 45 % is attained. However, ~~this~~ the DOT500 allows for prototyping, and provides a proof of concept for faster development towards the ideal DOT concept. From this point onwards, all discussions and calculations will refer to the intermediate DOT500 set-up, including the described oil circuit ~~(Diepeveen et al., 2018a)~~(Diepeveen et al., 2018b). A prototype was erected in June 2016 at Rotterdam Maasvlakte II, the Netherlands.

2.2 Drivetrain component specification

~~A~~ The drivetrain component specifications are summarized in Table 1 and a schematic overview and photograph of the DOT500 set-up is presented in Figure 3. An exhaustive description of the component matching process for the DOT500 is described in (Diepeveen, 2013). The components are described according to the enumerated labels in the figure~~, and the drivetrain components specifications are summarized in Table 1~~ :

Table 1. Hydraulic oil pump, oil motor and water pump specifications (Hägglunds, 2015; Bosch-Rexroth, 2012; KAMAT, 2017)

Description	Oil pump	Oil motor	Water pump
Brand and type	Hägglunds CB840	Bosch-Rexroth A6VLM	Kamat K80120G-5M
Volumetric displacement	52.8 l rev^{-1}	1.0 l rev^{-1}	2.3 l rev^{-1}
Nominal speed	32 rev min^{-1}	1600 rev min^{-1}	1500 rev min^{-1}
Torque range available	0 - 280 kNm	0 - 5571 Nm	0 - 5093 Nm
Pressure range available	0 - 350 bar	0 - 350 bar	0 - 125 bar
Power range available	0 - 870 kW	0 - 933 kW	0 - 800 kW
Torque range applied	0 - 210 kNm	0 - 3000 Nm	0 - 3000 Nm
Pressure range applied	0 - 230 bar	0 - 230 bar	0 - 70 bar

1. **Oil pump:** The rotor drives a Hägglunds CB840, which is a fixed-displacement radial piston motor. The motor is used here as pump and ~~will be~~ is referred to as the oil pump in the remainder of this paper. The pump is supplied with ~~a~~ sufficient flow and constant feed pressure ~~and flow~~ of 21 bar to keep the ~~pistons~~ piston bearings in continuous contact with the cam ring (Hägglunds, 2015). Load-pins are integrated in the suspension of the pump in the nacelle ~~, which enables measurement of~~ to measure the pump torque.
2. **Oil motor:** The high-pressure hydraulic discharge line of the oil pump drives a Bosch-Rexroth A6VLM variable-displacement axial piston oil motor ~~. The volumetric displacement can be adjusted by a built-in servo (Bosch-Rexroth, 2012) . However, in the considered set-up the device is configured to act as a fixed-displacement oil motor, as the DOT concept does not consider variable-displacement components~~(Bosch-Rexroth, 2012), configured here with a (maximum) fixed displacement.
3. **Water pump:** The oil motor is mechanically coupled to a Kamat K80120-5G fixed-displacement water plunger pump (KAMAT, 2017). An external centrifugal pump supplies the water pump with sufficient flow and ~~a constant feed pressure~~ feed pressure of around 2.6 bar.
4. **Spear valve:** The pressure in the water pump discharge line is controlled by variable-area orifices in the form of two spear valves. The valves are used to control the system torque and rotor speed in below- and near-rated operating conditions, and form high-speed water jets towards the Pelton turbine. A schematic visualization of this system is shown in Figure 4. The spear positions are measured and individually actuated by DC-motors~~, and are measured by resistive potentiometers~~.

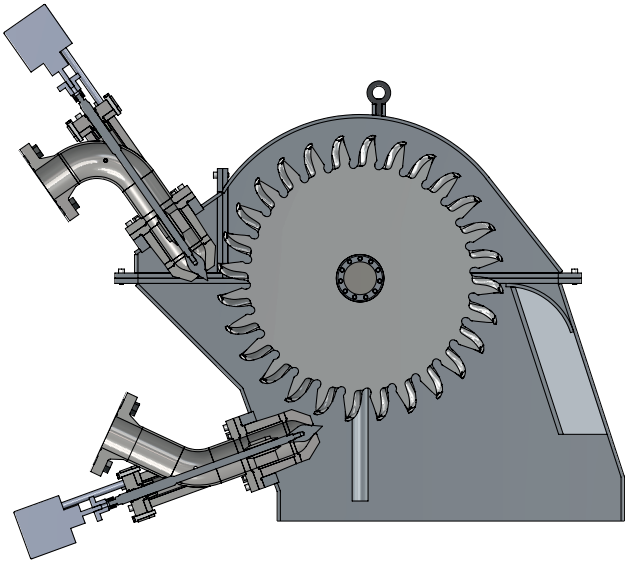

Figure 4. The pressurized hydrostatic water flow is converted to a hydrodynamic water jet using spear valves. The high-speed jets exert a force on the buckets of the Pelton turbine.

The spear valves are actuated in such a way ~~,~~that only full on-off spear position actuation is possible. This means that either the spear moves forwards or backwards at full speed, or the spear valve position remains at its current position. A deadband logic-controller is implemented to enable position control of the valve within a predefined band around the set point.

5. **Pelton turbine:** When the water flow exits the spear ~~valve~~valves, the hydrostatic energy in the high-pressure line is converted to a hydrodynamic high-velocity water jet. The momentum of the jet exerts a force on the Pelton turbine buckets (Zhang, 2007). Pelton turbines are highly specialized pieces of equipment and are designed to meet specific conditional requirements (Brekke, 2001). The Sy Sima 315 MW turbine in Norway, for 88.5 bar of head pressure is to date the largest known (Cabrera et al., 2015). The custom manufactured Pelton turbine employed in the DOT500 set-up is designed for the nominal pressure and the optimal speed conditions of the connected electrical generator.
   The Pitch Circle Diameter (PCD) of the custom manufactured wheel is 0.85 m and the nominal speed of the turbine is in the range of $1230 - 1420$ rpm. According to the manufacturer, the optimal operational pressure is in the range of $60 - 80$ bar for a nominal flow of approximately $58\,\mathrm{l\,min^{-1}}$ using two spear valves. The optimal ratio between the tangential Pelton and water jet speed is approximately $1/2$ (Thake, 2000), and is maintained by speed control of the asynchronous generator using a filtered pressure measurement. Further considerations on optimal Pelton operation under varying conditions are given below.
6. **Generator:** The mechanical rotational energy of the Pelton turbine is harvested by a mechanically coupled generator. As a grid connection was unavailable at the test location, the electrical energy excess is dissipated by a brake resistor.

In addition to the components described in the above-given enumeration, auxiliary hardware is present and required for operation of the turbine. A more detailed description is presented in (Diepeveen et al., 2018b), however, a short summary of the relevant components and remarks is given:

- **Cooling system:** Because of the significant mechanical losses, the working medium needs to be cooled to enable long-term operation of the turbine. The pump and motor in the oil circuit are equipped with flushing lines, which lead to the oil reservoir. A parallel forced-convection cooling circuit regulates the oil temperature.
- **Water circuit:** After the high-velocity water jet has hit the Pelton buckets, it falls back into the first water reservoir. A second water reservoir is connected to the first by a high-volume line to prevent a disturbed flow to the water pump. From the second reservoir the water is fed to the water pump by a centrifugal pump. The high-pressure circuit includes a pressure-relief valve.

Furthermore, a remark has to be made on the operational strategy of the Pelton turbine. It is concluded from earlier tests and manufacturer data sheets that Pelton efficiency characteristics are mainly a function of flow, and to a lesser extend of line pressure. The flow to the Pelton turbine is proportional to the wind turbine rotor speed, which results in suboptimal operation of the Pelton. The Pelton speed control strategy described above aims to extract the maximum amount of energy, given the conditions it is subjected to. For now, this is a design choice, and further research needs to be conducted to elaborate on Pelton design and efficiency maximization given the varying operational conditions.

3 Theory and model derivation of the hydraulic drivetrain

The theory for model derivation of the DOT500 hydraulic drivetrain is presented in this section. As control actions influence the turbine operating behavior to the point where the hydrodynamic water jet exits the spear valve, modeling of the turbine drivetrain ~~will be~~ is performed up to that point. After the water flow exits the spear valve, the aim to operate the Pelton turbine-generator combination at maximum efficiency is a decoupled control objective from the rest of the drivetrain~~, and is outside the scope of this paper~~. Considerations on this aspect are given in Section 2.2.

A simplified hydraulic diagram of the set-up is given in Figure 5. The components considered in the model derivation are shown in black, whereas auxiliary systems are presented in gray. The symbols in this figure are specified throughout the different parts of this section. In this section, pressures are generally given as a pressure difference Δp over a component, but when the pressure with respect to the atmospheric pressure p_0 is intended, the Δ-indication is omitted.

The organization is divided in two parts. First, a steady-state drivetrain model is derived in Sect. 3.1. This model is used later for derivation of a passive torque control strategy. Secondly, in Sect. 3.2, a drivetrain model including oil line dynamics is derived, and is used for design of an active spear valve control strategy.

3.1 Steady-state drivetrain modeling

A steady-state model of the drivetrain is derived for hydraulic torque control design in below-rated operating conditions. Mathematical models of hydraulic wind turbines have been established, but mostly incorporate a drivetrain with variable dis-

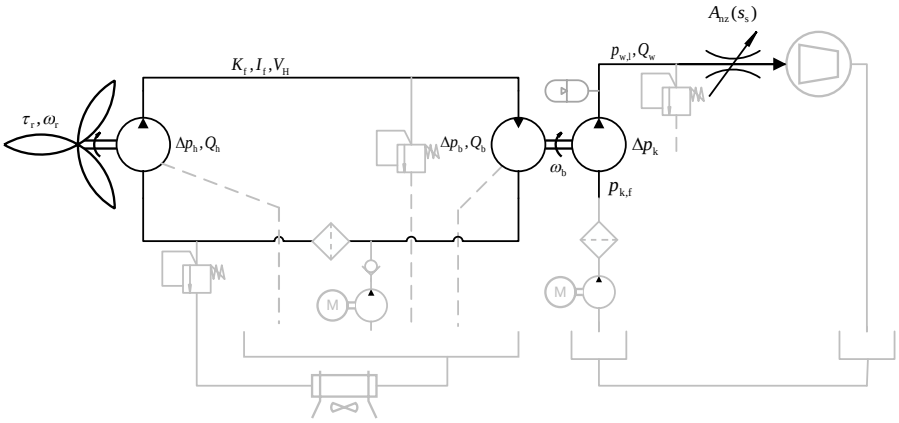

Figure 5. Schematic overview of the DOT500 hydraulic wind turbine drivetrain. All pumps and motors have a fixed volume displacement. Charge pressure pumps and filters are included on the low-pressure sides of both the oil and water circuits. Pressure relief valves are incorporated in both circuits. A parallel circuit around the oil reservoir is present for cooling purposes.

placement components (Buhagiar et al., 2016; Jarquin Laguna, 2017). In (Skaare et al., 2011, 2013) a more simple, robust and efficient drivetrain with discrete hydraulic gear ratio is proposed, by enabling and disabling hydraulic motors. Recently, a feedback control strategy for wind turbines with digital fluid power transmission is described in (Pedersen et al., 2017). However, only fixed-displacement components are considered and modeling of such a DOT drivetrain is described in (Diepeveen, 2013). The model derivation in this section incorporates the components employed in the actual DOT500 set-up. A simplified wind turbine model is introduced in Sect. 3.1.1. This model is complemented in Sect. 3.1.2 by analytic models of drivetrain components.

3.1.1 Simplified wind turbine model

The Newton law for rotational motion is employed as a basis for modeling the wind turbine rotor speed dynamics

$$J_r \dot{\omega}_r = \tau_r - \tau_{sys}, \tag{1}$$

where J_r is the rotor inertia, ω_r the rotor rotational speed, τ_r the mechanical torque supplied by the rotor to the low-speed shaft, and τ_{sys} the system torque supplied by the hydraulic oil pump to the shaft. The rotor inertia J_r of the rotor is not publicly available. However, an estimation of the rotor inertia is obtained using an empiric relation on blade length given in (Rodriguez et al., 2007), resulting in a value of ~~$6.6 \cdot 10^5$~~ $6.6 \cdot 10^5$ kg m^2. Moreover, experiments were performed on the actual turbine and confirm this theoretical result (Jager, 2017). The torque supplied by the rotor (Bianchi et al., 2006) is given by

$$\tau_r = \frac{1}{2} \rho_{air} \pi R^3 U^2 C_p(\lambda, \beta)/\lambda, \tag{2}$$

where the density of air ρ_{air} is taken as a constant value of ~~1.225~~1.225 kg m^{-3}, U is the velocity of the upstream wind, and R is the blade length of ~~22~~22 m. The power coefficient C_p represents the fraction between the captured rotor power P_r and the

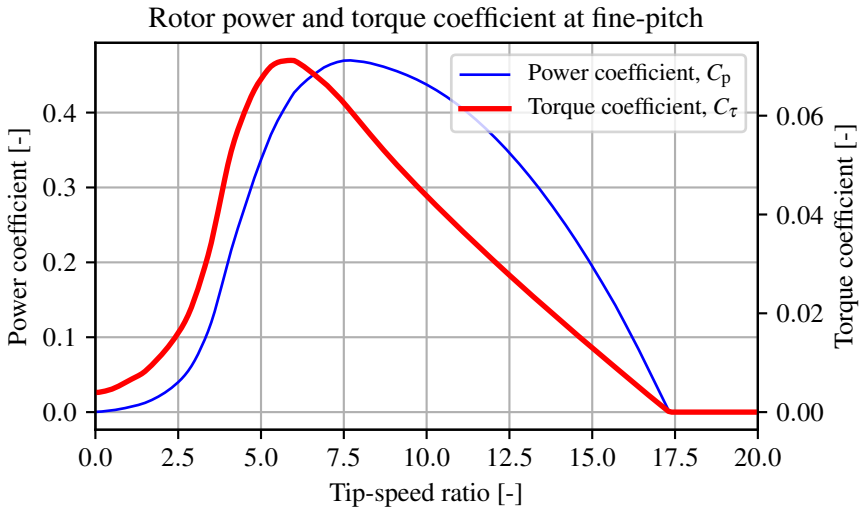

Figure 6. Rotor power and torque coefficient curve of the rotor, obtained from a BEM analysis performed on measured blade-geometry data. The maximum power coefficient $C_{\mathrm{p,max}}$ of 0.48 is attained at a tip-speed ratio of 7.8. The maximum torque coefficient of $C_{\tau,\mathrm{max}}$ is given by $7.2 \cdot 10^{-2}$ at a lower tip-speed ratio of 5.9.

available wind power P_{wind}, and is a function of the blade pitch angle β and the dimensionless tip-speed ratio λ given by

$$\lambda = \omega_{\mathrm{r}} R / U. \tag{3}$$

The power coefficient C_{p} is related to the torque coefficient

$C_\tau(\lambda,\beta) = C_{\mathrm{p}}(\lambda,\beta)/\lambda,$

by $C_\tau(\lambda,\beta) = C_{\mathrm{p}}(\lambda,\beta)/\lambda$ such that Eq. (2) can be rewritten as

$$\tau_{\mathrm{r}} = \frac{1}{2}\rho_{\mathrm{air}}\pi R^3 U^2 C_\tau(\lambda,\beta). \tag{4}$$

The rotor power and torque extraction capabilities from the wind are characterized in respective power and torque coefficient curves. These curves of the actual DOT500 rotor are generated by mapping the actual blade airfoils, and applying Blade Element Momentum (BEM) theory (Burton et al., 2011), and are given in Figure 6 at the blade fine-pitch angle. The fine-pitch angle β_0 indicates the blade angle resulting in maximum rotor power extraction in the below-rated operating region (Bossanyi, 2000). The theoretical maximum rotor power and torque coefficients equal $C_{\mathrm{p,max}} = 0.48$ and $C_{\tau,\mathrm{max}} = 7.2 \cdot 10^{-2}$, at tip-speed ratios of 7.8 and 5.9, respectively. The complete power, torque and thrust coefficient data set is available as an external supplement under (Mulders et al., 2018b).

The system torque τ_{sys} is supplied by the hydraulic drivetrain to the rotor low-speed shaft. This torque is influenced by the components in the drivetrain, which all have their own energy conversion characteristics expressed in efficiency curves. All

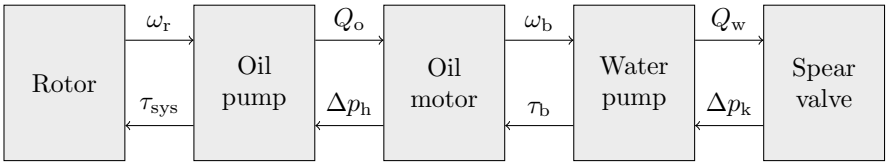

Figure 7. Flow diagram of the DOT500 hydraulic drivetrain. For steady-state modeling purposes, first the flow path is calculated up to the spear valve. The effective nozzle area and the water flow through the spear valve determine the hydraulic feed line pressure, which influences the system torque τ_{sys} to the rotor.

components are off-the-shelf and their combined efficiency characteristics influence the operating behavior of the turbine. ~~As hydraulic~~

Hydraulic components are known for their high torque-to-inertia ratio, ~~this results in~~ and have high acceleration capabilities ~~(Merritt, 1967). Therefore, it is assumed in this paper that the pumps and motor included in the drivetrain have negligible dynamics, and the power conversion (flow-speed, torque-pressure) is given by static relations. This assumption is supported by an analysis~~ as a result (Merritt, 1967). In typical applications of a hydraulic transmission, the fairly low rotational inertia of pumps and motors is still relevant. However, the considered wind turbine drivetrain is driven by a rotor with a large inertia J_r compared to the drivetrain components. Referring to the specification sheet of the oil motor (Bosch-Rexroth, 2012), it is stated that the unit has a moment of inertia of $J_b = 0.55\,\mathrm{kg\,m^2}$. The resulting reflected inertia to the rotor of $J_{b\to r} = 0.55/G^2 = 1533.312\,\mathrm{kg\,m^2}$ is still negligible, where G^{-1} represents the *hydraulic gear ratio* of 52.8. Furthermore, a particular study on this aspect has been carried out in ~~(Kempenaar, 2012; Diepeveen, 2013)~~(Kempenaar, 2012), where it is concluded that inclusion of component dynamics does not result in significantly improved model accuracy. For the reasons mentioned, the pumps and motor included in the drivetrain are assumed to have negligible dynamics, and the power conversion (flow-speed, torque-pressure) is given by static relations.

3.1.2 Analytic drivetrain components description

A flow diagram of the modeling strategy is presented in Figure 7. To obtain an expression for the system torque τ_{sys}, the complete hydraulic flow path with its volumetric losses is modeled first. When the flow path reaches the spear valve at the water discharge to the Pelton turbine, the simulation path is reversed to calculate the effect of all component characteristics to the line pressures. The spear valve allows for control of the water discharge pressure, of which the effect propagates back to the system torque τ_{sys}. The high-pressure oil flow by the oil pump is proportional to the rotor speed

$$Q_o = V_{p,h}\omega_r\eta_{v,h}, \tag{5}$$

where the $V_{p,h}$ is the pump volumetric displacement, and $\eta_{v,h}$ the volumetric efficiency. The volumetric efficiency indicates the volume loss as a fraction of the total displaced flow ~~, and decreases as the pressure increases~~as function of the component operating conditions. However, ~~the volumetric efficiency of a pump or motor is generally high and fairly constant over the~~

~~entire operating range (Diepeveen, 2013; Trostmann, 1995). Therefore~~as volumetric efficiency data is unavailable for most of the components and the aim is to provide a simplified model of the hydraulic drivetrain, volumetric losses ~~will be taken constant in this paper~~are considered as a constant factor of the displaced flow. The resulting oil flow Q_o drives the oil motor, which result in a rotational speed of the motor shaft subject to volumetric losses

$$\omega_\mathrm{b} = \frac{Q_\mathrm{o}}{V_\mathrm{p,b}} \eta_\mathrm{v,b}, \tag{6}$$

where $V_\mathrm{p,b}$ is the oil motor volumetric displacement, and $\eta_\mathrm{v,b}$ the volumetric efficiency of the oil motor. As the water pump is mechanically coupled to the oil motor axis, its rotational speed is equal to ω_b. The expression relating the rotational speed to the water pump discharge water flow Q_w is given by

$$Q_\mathrm{w} = V_\mathrm{p,k} \omega_\mathrm{b} \eta_\mathrm{v,k}, \tag{7}$$

where $V_\mathrm{p,k}$ is the volumetric displacement of the water pump, and $\eta_\mathrm{v,k}$ the volumetric efficiency of the water pump. The pressure in the water discharge line is controlled by a spear valve of which a visualization is given in Figure 8, with the spear position coordinate system. The effective nozzle area is variable according to the relation

$$A_\mathrm{nz}(s) = N_\mathrm{s} \pi \left(D_\mathrm{nz}^2/4 - (s_\mathrm{max} - s)^2 \tan^2(\alpha/2) \right), \tag{8}$$

where $\{s \subset \mathbb{R} \mid 0 \leq s \leq s_\mathrm{max}\}$ represents the position of the spear in the circular nozzle cross-section, D_nz is the nominal nozzle diameter, α the spear coning angle, and N_s indicates the amount of spear valves on the same line. Modeling multiple spear valves by N_s assumes equal effective nozzle areas for all valves. The maximum spear position (fully open) is given by

$$s_\mathrm{max} = \frac{D_\mathrm{nz}}{2 \tan(\alpha/2)}. \tag{9}$$

and a mapping for spear position to effective nozzle area for different nozzle diameters D_nz is given in Figure 9. The spear valve is closed for all cases at position ~~$s = 0$ mm.~~ $s = 0$ mm. The spear valve converts the hydrostatic water flow into a high-speed hydrodynamic water jet, that exerts a thrust force on the buckets of the Pelton turbine (Zhang, 2007). ~~To describe this energy conversion,~~ Using the Bernoulli equation for incompressible flows (White, 2011)~~is used~~

$$\frac{1}{2}\rho_\mathrm{w} v_\mathrm{w,l}^2 + \rho_\mathrm{w} g z_\mathrm{w,l} + p_\mathrm{w,l} \quad = \tfrac{1}{2}\rho_\mathrm{w} v_\mathrm{w,nz}^2 + \rho_\mathrm{w} g z_\mathrm{w,nz} + p_\mathrm{w,nz},$$

~~where v_w represents the water velocity, p_w the water pressure, and the subscripts $(\cdot)_\mathrm{w,l}$ and $(\cdot)_\mathrm{w,nz}$ indicate the locations before and after the nozzle, respectively. As in the given control volume the height difference Δz equals zero, and the water density ρ_w and gravitational constant g are constant, the potential term is disregarded. Using Eq.~~, an expression for the discharge water pressure ~~$p_\mathrm{w,l}$~~ is obtained

$$p_\mathrm{w,l}(s) = \frac{\rho_\mathrm{w}}{2} \left(\frac{Q_\mathrm{w}}{C_\mathrm{d} A_\mathrm{nz}(s)} \right)^2, \tag{10}$$

where the flow and effective nozzle area $\{Q_\mathrm{w}, A_\mathrm{nz}\} \subset \mathbb{R}^+$. As observed in the above given relation, the pressure can be controlled by varying the feed flow and spear position, as the latter influences the effective nozzle area A_nz. The discharge

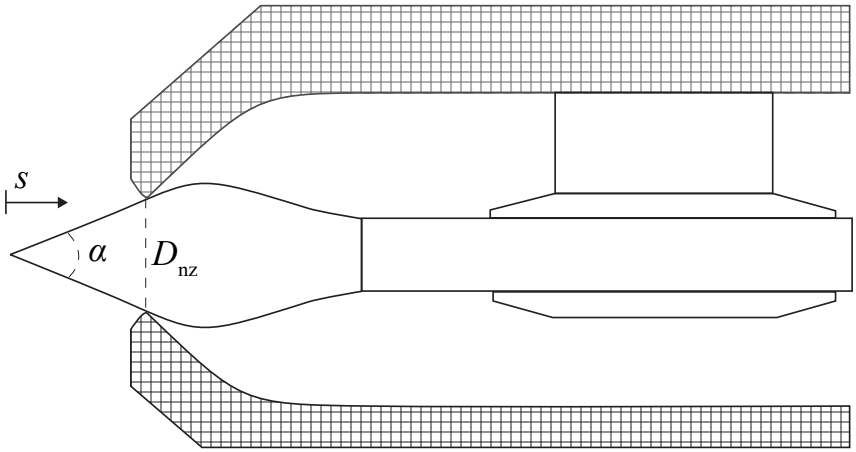

Figure 8. Cross-section of the spear valve used. The coning angle of the spear is given by α, the nozzle diameter by D_{nz}, and the position of the spear tip in the nozzle by s. The nozzle heads are adjustable for adjustment of the outlet area.

coefficient C_{d} is introduced to account for pressure losses due to the geometry and flow regime at the nozzle exit (Al'tshul' and Margolin, 1968). The discharge coefficient of an orifice is defined as the ratio between the vena contracta area and the orifice area (Bragg, 1960). The vena contracta is the point where the streamlines become parallel, which usually occurs downstream of the orifice where the streamlines are still converging.

The pressure in the water discharge line propagates back into the system ~~, and can be~~ and is used as a substitute to conventional wind turbine torque control. A relation for the mechanical torque at the axis between the water pump and oil motor is given by

$$\tau_{\mathrm{b}} = \frac{V_{\mathrm{p,k}} \Delta p_{\mathrm{k}}}{\eta_{\mathrm{m,k}}(\omega_{\mathrm{b}}, \Delta p_{\mathrm{k}})}, \tag{11}$$

where $\eta_{\mathrm{m,k}}$ is the mechanical efficiency of the water pump as function of the rotational speed and pressure difference over the pump

$$\Delta p_{\mathrm{k}} = p_{\mathrm{w,l}} - p_{\mathrm{k,f}}, \tag{12}$$

where $p_{\mathrm{k,f}}$ is a known and constant feed pressure. The torque τ_{b} is used to calculate the pressure difference over the oil motor and pump by

$$\Delta p_{\mathrm{b}} = \Delta p_{\mathrm{h}} = \frac{\tau_{\mathrm{b}}}{V_{\mathrm{p,b}} \eta_{\mathrm{m,b}}(\omega_{\mathrm{b}}, \tau_{\mathrm{b}})}, \tag{13}$$

where $\eta_{\mathrm{m,b}}$ is the mechanical efficiency of the oil motor. It is assumed that the pressure at the discharge outlet of the oil motor Δp_{b} is constant as the feed pressure to the oil pump is regulated. Finally, the system torque supplied to the rotor low-speed

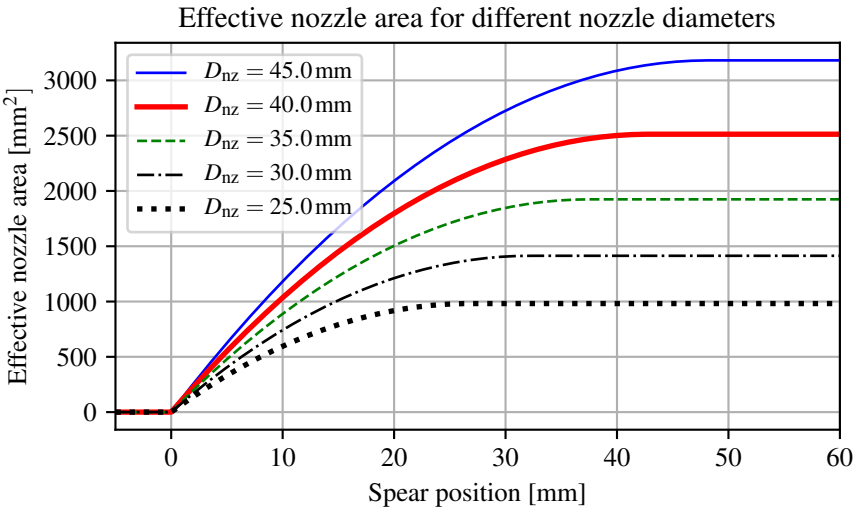

Figure 9. Effective nozzle area as function of the spear position in the circular nozzle cross-section. The spear valve is fully closed at ~~$s = 0$~~ $s = 0$ mm and fully opened at $s = s_{max}$, of which the latter is variable according to the nozzle head diameter.

shaft is given by

$$\tau_{sys} = \frac{V_{p,h}\Delta p_h}{\eta_{m,h}(\omega_r, \Delta p_h)}. \tag{14}$$

Using the relations derived, a passive strategy for below-rated turbine control is presented in Sect. 4.1.

3.2 Dynamic drivetrain modeling

In contrast to the steady-state model presented previously, this section elaborates on the derivation of a drivetrain model including fluid dynamics for validation of the control design in the near-rated region. First, preliminary knowledge on fluid dynamics is given in Sect. 3.2.1, whereafter a dynamic DOT500 drivetrain model is presented in Sect. 3.2.2.

3.2.1 Analysis of fluid dynamics in a hydraulic line

The dynamics of a volume in a hydraulic line are modeled in this section. For this, analogies between mechanical and hydraulic systems are employed for modeling convenience. A full derivation is given in Appendix B, only the results are given in this section. The system considered, representing the high-pressure discharge oil line, is a cylindrical control volume $V_H = AL_l = \pi r_l^2 L_l$, with radius r_l and length L_l, excited by a pressure $\Delta p = p_{in} - p_{out}$. The net flow into the control volume is defined as $Q = Q_{in} - Q_{out}$. ~~First, the differential equation for a standard mass-damper-spring system driven by an external force F is given by~~

$F = m\ddot{x} + c\dot{x} + kx.$

~~For conversion to a hydraulic equivalent expression , the driving mechanical force is substituted by $F = \Delta pA$, the control volume mass is taken as $m = \rho V_{\mathrm{H}} = \rho A L_{\mathrm{l}}$, and the fluid inflow velocity defined as $\dot{x} = Q/A$. By rearranging terms~~For a hydraulic expression with pressure Δp as the external excitation input and the flow Q as output, one obtains

$$\Delta p = \frac{\rho L_{\mathrm{l}}}{A}\dot{Q} + \frac{c}{A^2}Q + \frac{k}{A^2}\int Q dt,$$

~~which is further simplified into~~

$$\Delta p = L_{\mathrm{H}}\dot{Q} + R_{\mathrm{H}}Q + \frac{1}{C_{\mathrm{H}}}\int Q dt, \tag{15}$$

where L_{H}, R_{H} and C_{H} are the hydraulic induction, resistance and capacitance (Esposito, 1969), respectively, and are defined in Appendix A. The ~~former two of these three quantities depend on the flow Reynolds number, which shows whether the inertial or viscosity terms are dominant in the Navier-Stokes equations (Merritt, 1967). The Reynolds number is defined as~~

$$Re = \frac{D_{\mathrm{l}} v \rho}{\mu},$$

~~where $D_{\mathrm{l}} = 2r_{\mathrm{l}}$ is the line diameter, and μ the fluid dynamic viscosity. For Reynolds numbers larger than 4000 the flow is considered as turbulent and the inertial terms are dominant, whereas for values smaller than 2300 the viscosity terms are deemed dominant.~~

~~For evaluation of the natural frequency ω_{n} and damping ratio ζ for the considered system, the characteristic equation by neglecting the external excitation force ($\Delta p = 0$) is defined as~~

$$0 = \dot{Q} + \frac{R_{\mathrm{H}}}{L_{\mathrm{H}}}Q + \frac{1}{C_{\mathrm{H}}L_{\mathrm{H}}}\int Q dt \tag{16}$$

$$= \dot{Q} + 2\zeta\omega_{\mathrm{n}}Q + \omega_{\mathrm{n}}^2\int Q dt. \tag{17}$$

~~Evaluating the quantities ω_{n} and ζ, results in~~

$$\omega_{\mathrm{n}} = \sqrt{\frac{1}{C_{\mathrm{H}}L_{\mathrm{H}}}},$$

$$\zeta_{\mathrm{p}} = \frac{R_{\mathrm{H}}}{2}\sqrt{\frac{C_{\mathrm{H}}}{L_{\mathrm{H}}}}.$$

~~The~~ inverse result of Eq. (15) is obtained (Murrenhoff, 2012) ~~,~~ with flow Q as the external excitation and Δp as output

$$Q = C_{\mathrm{H}}\Delta\dot{p} + \frac{1}{R_{\mathrm{H}}}\Delta p + \frac{1}{L_{\mathrm{H}}}\int \Delta p dt. \tag{18}$$

~~Now by evaluating the characteristic equation~~

$$0 = C_{\mathrm{H}}\Delta\dot{p} + \frac{1}{R_{\mathrm{H}}}\Delta p + \frac{1}{L_{\mathrm{H}}}\int \Delta p dt \tag{19}$$

$$= \Delta\dot{p} + \frac{1}{R_{\mathrm{H}}C_{\mathrm{H}}}\Delta p + \frac{1}{L_{\mathrm{H}}C_{\mathrm{H}}}\int \Delta p dt, \tag{20}$$

~~and using Eq. , it is seen that the natural frequency remains unchanged with the result obtained in Eq. , but the definition of the damping ratio changes~~

$\zeta_{\mathrm{Q}} = \frac{1}{2R_{\mathrm{H}}}\sqrt{\frac{L_{\mathrm{H}}}{C_{\mathrm{H}}}}$.

Finally, the differential equation defined by Eq. (15) is expressed as a transfer function ~~in~~

$$G_{\mathrm{Q}/\Delta\mathrm{p}}(s) = \frac{1/L_{\mathrm{H}}}{s + (R_{\mathrm{H}}/L_{\mathrm{H}}) + 1/(C_{\mathrm{H}}L_{\mathrm{H}}s)} = \frac{s/L_{\mathrm{H}}}{s^2 + (R_{\mathrm{H}}/L_{\mathrm{H}})s + 1/(C_{\mathrm{H}}L_{\mathrm{H}})}, \tag{21}$$

and the same is done for Eq. (18)

$$G_{\Delta\mathrm{p}/\mathrm{Q}}(s) = \frac{1/C_{\mathrm{H}}}{s + 1/(R_{\mathrm{H}}C_{\mathrm{H}}) + 1/(C_{\mathrm{H}}L_{\mathrm{H}}s)} = \frac{s/C_{\mathrm{H}}}{s^2 + 1/(R_{\mathrm{H}}C_{\mathrm{H}})s + 1/(C_{\mathrm{H}}L_{\mathrm{H}})}. \tag{22}$$

The transfer functions defined in ~~Eq.s~~Eqs. (21) and (22) show the characteristics of an inverted notch with $+1$ and -1 slopes on the left and right side of the natural frequency, respectively. This physically means that exciting the system pressure results in a volume velocity change predominantly at the system natural frequency for the former mentioned case~~, and vice versa for the latter mentioned.~~ . An illustrative Bode plot is given in Sect. 4.2.1. Exciting the flow results in amplification/transmission to pressure in a wider frequency region. This effect is a result of the inverse proportionality between the damping coefficients ζ_{Q} and ζ_{p} (see Appendix B).

3.2.2 Drivetrain model derivation

A dynamic model of the DOT500 drivetrain is derived by application of the theory presented in the previous section. The drivetrain is defined from the rotor up to the spear valve, and the following assumptions are made:

- Because of the high torque to inertia ratio of hydraulic components (Merritt, 1967), the dynamics of oil pumps and motors are disregarded and taken as analytic relations;
- Because of the longer line length and higher compressibility of oil compared to the shorter water column, the high-pressure oil line is more critical for control design, and a dynamic model ~~will be~~ is implemented for this column only;
- ~~Hydraulic lines are modeled as being rigid;~~
- The fluids have a constant temperature.

The dynamic system is governed by the following differential equations

$$\mathcal{V} = \mathcal{V}_{\mathrm{in}} - \mathcal{V}_{\mathrm{out}}, \qquad \dot{\mathcal{V}} = Q = Q_{\mathrm{in}} - Q_{\mathrm{out}}, \tag{23}$$

$$\Delta p_{\mathrm{h}} = \underbrace{\left(\frac{J_{\mathrm{r}}\eta_{\mathrm{m,h}}}{V_{\mathrm{p,h}}^2\eta_{\mathrm{v,h}}} + L_{\mathrm{H}}\right)}_{L_{\mathrm{R}}^*}\dot{Q}_{\mathrm{in}} + R_{\mathrm{H}}(Q_{\mathrm{in}} - Q_{\mathrm{out}}) + \frac{K_{\mathrm{f}}}{V_{\mathrm{H}}}\frac{K_{\mathrm{e}}}{V_{\mathrm{H}}}(\mathcal{V}_{\mathrm{in}} - \mathcal{V}_{\mathrm{out}}) = L_{\mathrm{R}}^*\dot{Q}_{\mathrm{in}} + R_{\mathrm{H}}(Q_{\mathrm{in}} - Q_{\mathrm{out}}) + \frac{1}{C_{\mathrm{H}}}\mathcal{V}, \tag{24}$$

$$\Delta p_{\mathrm{b}} = L_{\mathrm{H}}\dot{Q}_{\mathrm{out}} + R_{\mathrm{H}}(Q_{\mathrm{out}} - Q_{\mathrm{in}}) + \frac{K_{\mathrm{f}}}{V_{\mathrm{H}}}\frac{K_{\mathrm{e}}}{V_{\mathrm{H}}}(\mathcal{V}_{\mathrm{out}} - \mathcal{V}_{\mathrm{in}}) = L_{\mathrm{H}}\dot{Q}_{\mathrm{out}} + R_{\mathrm{H}}(Q_{\mathrm{out}} - Q_{\mathrm{in}}) - \frac{1}{C_{\mathrm{H}}}\mathcal{V}, \tag{25}$$

where K_e is the equivalent bulk modulus including the fluid and line compressibility defined in Eq. (A5), and $\mathcal{V}$ is the net volume inflow to the considered oil line, between the oil pump discharge and oil motor feed port. For convenience, mechanical model quantities are expressed hydraulically in terms of fluid flows and pressure differences over the components. Therefore, the rotor inertia J_r is expressed in terms of fluid induction, and is combined with the hydraulic induction term into L_R^*.

Both the spear position and pitch angle are modeled by a first-order actuator model

$$\dot{s} = \frac{1}{t_\mathrm{s}}(s_\mathrm{ref} - s), \tag{26}$$

$$\dot{\beta} = \frac{1}{t_\beta}(\beta_\mathrm{ref} - \beta), \tag{27}$$

where t_s and t_β are the time constant for the spear valve and pitch actuators, respectively, and the phase loss at the actuator bandwidth is assumed to account for actuation delay effects.

The above given dynamic equations are written in a state-space representation as

$$\begin{bmatrix} \dot{\mathcal{V}} \\ \dot{Q}_\mathrm{in} \\ \dot{Q}_\mathrm{out} \\ \dot{s} \\ \dot{\beta} \end{bmatrix} = \begin{bmatrix} 0 & 1 & -1 & 0 & 0 \\ -\frac{1}{C_\mathrm{H} L_\mathrm{R}^*} & -\frac{R_\mathrm{H}}{L_\mathrm{R}^*} & \frac{R_\mathrm{H}}{L_\mathrm{R}^*} & 0 & 0 \\ \frac{1}{C_\mathrm{H} L_\mathrm{H}} & \frac{R_\mathrm{H}}{L_\mathrm{H}} & -\frac{R_\mathrm{H}}{L_\mathrm{H}} & 0 & 0 \\ 0 & 0 & 0 & -\frac{1}{t_\mathrm{s}} & 0 \\ 0 & 0 & 0 & 0 & -\frac{1}{t_\beta} \end{bmatrix} \begin{bmatrix} \mathcal{V} \\ Q_\mathrm{in} \\ Q_\mathrm{out} \\ s \\ \beta \end{bmatrix} + \begin{bmatrix} 0 \\ \frac{1}{L_\mathrm{R}^*}\Delta p_\mathrm{h} \\ -\frac{1}{L_\mathrm{H}}\Delta p_\mathrm{b} \\ \frac{1}{t_\mathrm{s}} s_\mathrm{ref} \\ \frac{1}{t_\beta}\beta_\mathrm{ref} \end{bmatrix}. \tag{28}$$

It is seen that the pressure difference over the oil pump and motor appear as inputs, but these quantities cannot be controlled directly. For this reason, linear expressions of the rotor torque and spear valves are defined next. The rotor torque is linearized with respect to the tip-speed ratio, pitch angle and wind speed

$$\hat{\tau}_\mathrm{r}(\bar{\omega}_\mathrm{r}, \bar{\beta}, \bar{U}) = k_{\omega_\mathrm{r}}(\bar{\omega}_\mathrm{r}, \bar{\beta}, \bar{U})\hat{\omega}_\mathrm{r} + k_\beta(\bar{\omega}_\mathrm{r}, \bar{\beta}, \bar{U})\hat{\beta} + k_\mathrm{U}(\bar{\omega}_\mathrm{r}, \bar{\beta}, \bar{U})\hat{U}, \tag{29}$$

where $\hat{(\cdot)}$ indicates a value deviation from the operating point, and $\bar{(\cdot)}$ is the value at the operating point (Bianchi et al., 2006). Furthermore,

$$k_{\omega_\mathrm{r}}(\omega_\mathrm{r}, \beta, U) = \frac{\partial \tau_\mathrm{r}}{\partial \omega_\mathrm{r}} = c_\mathrm{r} R U \frac{\partial C_\tau(\omega_\mathrm{r} R/U, \beta)}{\partial \lambda}, \tag{30}$$

$$k_\beta(\omega_\mathrm{r}, \beta, U) = \frac{\partial \tau_\mathrm{r}}{\partial \beta} = c_\mathrm{r} U^2 \frac{\partial C_\tau(\omega_\mathrm{r} R/U, \beta)}{\partial \beta}, \tag{31}$$

$$k_\mathrm{U}(\omega_\mathrm{r}, \beta, U) = \frac{\partial \tau_\mathrm{r}}{\partial U} = 2 c_\mathrm{r} U C_\tau(\omega_\mathrm{r} R/U, \beta) + c_\mathrm{r} U^2 \frac{\partial C_\tau(\omega_\mathrm{r} R/U, \beta)}{\partial \lambda} \frac{\partial \lambda}{\partial U} \tag{32}$$

$$= 2 c_\mathrm{r} U C_\tau(\omega_\mathrm{r} R/U, \beta) - c_\mathrm{r} \omega_\mathrm{r} R \frac{\partial C_\tau(\omega_\mathrm{r} R/U, \beta)}{\partial \lambda}, \tag{33}$$

$$c_\mathrm{r} = \frac{1}{2}\rho \pi R^3, \tag{34}$$

where the quantities k_{ω_r}, k_β and k_U represent the intrinsic speed feedback gain, the linear pitch gain and the linear wind speed gain, respectively. The intrinsic speed feedback gain can also be expressed as a function of the tip-speed ratio by

$$k_\lambda(\lambda, \beta, U) = k_{\omega_\mathrm{r}}(\omega_\mathrm{r}, \beta, U)\frac{U}{R}. \tag{35}$$

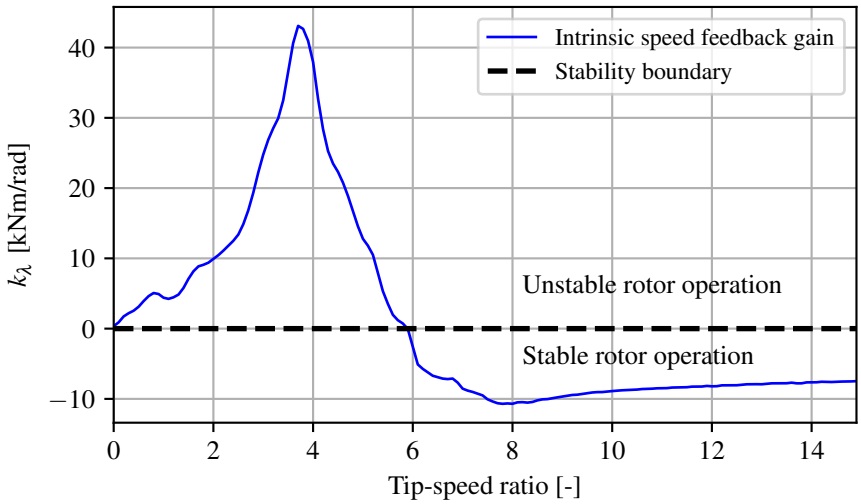

Figure 10. The intrinsic speed feedback gain $k_\lambda(\lambda, \bar{\beta}, \bar{U})$ as function of tip-speed ratio λ, at a fixed pitch angle and wind speed of ~~−2~~ −2 deg and ~~8~~8 m s^{-1}. Stable turbine operation is attained for non-positive values of k_λ.

For aerodynamic rotor stability, the value of k_λ needs to be negative. In Figure 10 the intrinsic speed feedback gain $k_\lambda(\lambda, \bar{\beta}, \bar{U})$ is evaluated as a function of the tip-speed ratio at the fine-pitch angle β_0. For incorporation of the linearized rotor torque in the drivetrain model, Eq. (29) is expressed in the pressure difference over the oil pump

$$\Delta\hat{p}_\mathrm{h}(\bar{\omega}_\mathrm{r}, \bar{\beta}, \bar{U}) = k^*_{\mathrm{Q_{in}}}(\bar{\omega}_\mathrm{r}, \bar{\beta}, \bar{U})\hat{Q}_\mathrm{in} + k^*_\beta(\bar{\omega}_\mathrm{r}, \bar{\beta}, \bar{U})\hat{\beta} + k^*_\mathrm{U}(\bar{\omega}_\mathrm{r}, \bar{\beta}, \bar{U})\hat{U}, \tag{36}$$

where the conversions of the required quantities are given by

$$k^*_{\mathrm{Q_{in}}} = k_{\omega_\mathrm{r}} \frac{\eta_\mathrm{m,h}}{V^2_\mathrm{p,h}\eta_\mathrm{v,h}}, \qquad k^*_\beta = k_\beta \frac{\eta_\mathrm{m,h}}{V_\mathrm{p,h}}, \qquad k^*_\mathrm{U} = k_\mathrm{U} \frac{\eta_\mathrm{m,h}}{V_\mathrm{p,h}}. \tag{37}$$

Similarly, the water line pressure as defined in Eq. (10) is linearized with respect to the spear position and flow through the valve

$$\hat{p}_\mathrm{w,l}(\hat{Q}_\mathrm{w}, \hat{s}) = k_\mathrm{s,s}(\bar{Q}_\mathrm{w}, \bar{s})\hat{s} + k_{\mathrm{s,Q_w}}(\bar{Q}_\mathrm{w}, \bar{s})\hat{Q}_\mathrm{w}, \tag{38}$$

where

$$k_\mathrm{s,s}(\bar{Q}_\mathrm{w}, \bar{s}) = \left. \frac{2Q^2_\mathrm{w}\rho_\mathrm{w}(s - s_\mathrm{max})\tan^2(\alpha/2)}{C^2_\mathrm{d}N^2_\mathrm{s}\pi^2\left(D^2_\mathrm{nz}/4 - (s_\mathrm{max} - s)^2\tan^2(\alpha/2)\right)^3} \right|_{\bar{Q}_\mathrm{w}, \bar{s}}, \tag{39}$$

$$k_{\mathrm{s,Q_w}}(\bar{Q}_\mathrm{w}, \bar{s}) = \left. \frac{Q_\mathrm{w}\rho_\mathrm{w}}{C^2_\mathrm{d}N^2_\mathrm{s}\pi^2\left(D^2_\mathrm{nz}/4 - (s_\mathrm{max} - s)^2\tan^2(\alpha/2)\right)^2} \right|_{\bar{Q}_\mathrm{w}, \bar{s}}. \tag{40}$$

The pressure difference over the oil motor is defined in terms of the water line pressure which is a function of the spear position

$$\Delta\hat{p}_{\mathrm{b}} = \frac{1}{c_{\mathrm{m,bk}}}\Delta\hat{p}_{\mathrm{k}} \approx \frac{1}{c_{\mathrm{m,bk}}}\hat{p}_{\mathrm{w,l}}(s) = \frac{1}{c_{\mathrm{m,bk}}}\left(k_{\mathrm{s,s}}(\bar{Q}_{\mathrm{w}},\bar{s})\hat{s} + k_{\mathrm{s,Q_w}}(\bar{Q}_{\mathrm{w}},\bar{s})\hat{Q}_{\mathrm{w}}\right), \tag{41}$$

where the mechanical and volumetric conversion factors from oil to water pressure and flow are defined as

$$c_{\mathrm{m,bk}} = \frac{V_{\mathrm{p,b}}}{V_{\mathrm{p,k}}}\eta_{\mathrm{m,k}}\eta_{\mathrm{m,b}}, \qquad c_{\mathrm{v,bk}} = \frac{V_{\mathrm{p,k}}}{V_{\mathrm{p,b}}}\eta_{\mathrm{v,k}}\eta_{\mathrm{v,b}} \tag{42}$$

The system defined in Eq. (28) is now presented as a linear state-space system of the form

$$\begin{aligned}\dot{x} &= Ax + Bu + B_{\mathrm{U}}\hat{U}\\ y &= Cx,\end{aligned} \tag{43}$$

~~and by substitution~~ Substitution of the rotor torque and water pressure approximations defined ~~in Eq.s~~by Eqs. (36) and (41) in Eq. (28), the state A, input B, ~~input~~ wind disturbance B_{U} and output C matrices are given by

$$A = \begin{bmatrix} 0 & 1 & -1 & 0 & 0\\ -\frac{1}{C_{\mathrm{H}}L^*_{\mathrm{R}}} & -\frac{R_{\mathrm{H}}-k^*_{\mathrm{Q_{in}}}}{L^*_{\mathrm{R}}} & \frac{R_{\mathrm{H}}}{L^*_{\mathrm{R}}} & 0 & \frac{k^*_\beta}{L^*_{\mathrm{R}}}\\ \frac{1}{C_{\mathrm{H}}L_{\mathrm{H}}} & \frac{R_{\mathrm{H}}}{L_{\mathrm{H}}} & -\frac{1}{L_{\mathrm{H}}}\left(R_{\mathrm{H}} + \frac{c_{\mathrm{v,bk}}}{c_{\mathrm{m,bk}}}k_{\mathrm{s,Q_w}}\right) & -\frac{1}{c_{\mathrm{m,bk}}L_{\mathrm{H}}}k_{\mathrm{s,s}} & 0\\ 0 & 0 & 0 & -\frac{1}{t_{\mathrm{s}}} & 0\\ 0 & 0 & 0 & 0 & -\frac{1}{t_\beta} \end{bmatrix}, \qquad B = \begin{bmatrix} 0 & 0\\ 0 & 0\\ 0 & 0\\ \frac{1}{t_{\mathrm{s}}} & 0\\ 0 & \frac{1}{t_\beta} \end{bmatrix},$$

$$B_{\mathrm{U}} = \begin{bmatrix} 0\\ \frac{k^*_{\mathrm{U}}}{L^*_{\mathrm{R}}}\\ 0\\ 0\\ 0 \end{bmatrix}, \qquad C = \begin{bmatrix} 1 & 0 & 0 & 0 & 0\\ 0 & \frac{1}{V_{\mathrm{p,h}}\eta_{\mathrm{v,h}}} & 0 & 0 & 0\\ 0 & 0 & 0 & 1 & 0\\ 0 & 0 & 0 & 0 & 1 \end{bmatrix}, \tag{44}$$

with the state, input and output matrices

$$\begin{aligned} x &= \begin{bmatrix} \hat{\mathcal{V}} & \hat{Q}_{\mathrm{in}} & \hat{Q}_{\mathrm{out}} & \hat{s} & \hat{\beta} \end{bmatrix}^T,\\ u &= \begin{bmatrix} \hat{s}_{\mathrm{ref}} & \hat{\beta}_{\mathrm{ref}} \end{bmatrix}^T,\\ y &= \begin{bmatrix} \hat{\mathcal{V}} & \hat{\omega}_{\mathrm{r}} & \hat{s} & \hat{\beta} \end{bmatrix}^T. \end{aligned} \tag{45}$$

The dynamic model derived in this section is used in Sect. 4.2 to come up with an active spear valve torque control strategy in the near-rated region.

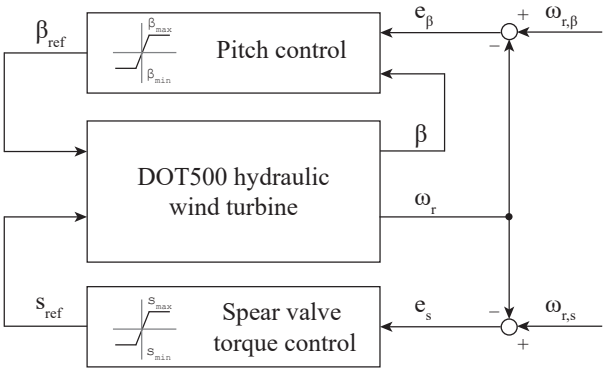

Figure 11. Schematic diagram of the DOT500 control strategy. When the control error e is negative, the controllers saturate at their minimum or maximum setting. In the near-rated operating region, the rotor speed is actively regulated to $\omega_{\mathrm{r,s}}$ by generating the spear position control signal s_{ref}, influencing the fluid pressure and the system torque. When the spear valve is at its rated minimum position, the gain-scheduled pitch controller generates a pitch angle set point β_{ref} to regulate the rotor speed at its nominal value $\omega_{\mathrm{r},\beta}$.

4 Controller design

In this section designs are presented for control in the below- and near-rated operating region. A schematic diagram of the overall control system is given in Figure 11. It is seen that the turbine is controlled by two distinct Proportional-Integral (PI) controllers, a spear valve torque and blade pitch controller, acting on individual rotor speed set point errors e_{s} and e_{β}, respectively. As both controllers have a common control objective of regulating the rotor speed and are implemented in a decentralized way, it is ensured that they are not active simultaneously. The gain-scheduled pitch controller is designed and implemented in a similar way as in conventional wind turbines (Jonkman et al., 2009), and is therefore not further elaborated in this paper. The spear valve torque controller, however, is non-conventional and its control design is outlined in this section.

For the below-rated control design a passive torque control strategy is employed, of which a description of is given in Sect. 4.1. Subsequently, in Sect. 4.2, the in-field active spear valve control implementation is evaluated using the dynamic drivetrain model.

4.1 Passive below-rated torque control

The passive control strategy for below-rated operation is described in this section. Conventionally, in below-rated operating conditions, the power coefficient is maximized by regulating the tip-speed ratio at λ_0 using generator torque control. Generally, the maximum power coefficient tracking objective is attained by implementing the feed-forward torque control law

$$\tau_{\mathrm{sys}} = \frac{\rho_{\mathrm{air}} \pi R^5 C_{\mathrm{p,max}}}{2\lambda^3} \omega_{\mathrm{r}}^2 = K_{\mathrm{r}} \omega_{\mathrm{r}}^2, \tag{46}$$

where K_{r} is the optimal mode gain in Nm (rad/s)$^{-2}$.

As the DOT500 drivetrain lacks the option to directly influence the system torque, hydraulic torque control is employed using spear valves. An expression for the system torque for the hydraulic drivetrain is derived by substitution of ~~Eq.s~~Eqs. (11) and (13) in Eq. (14)

$$\tau_{\mathrm{sys}} = \frac{V_{\mathrm{p,h}} V_{\mathrm{p,k}}}{V_{\mathrm{p,b}}} \frac{1}{\eta_{\mathrm{m,h}}(\omega_{\mathrm{r}}, \Delta p_{\mathrm{h}}) \eta_{\mathrm{m,b}}(\omega_{\mathrm{b}}, \tau_{\mathrm{b}}) \eta_{\mathrm{m,k}}(\omega_{\mathrm{b}}, \Delta p_{\mathrm{k}})} \Delta p_{\mathrm{k}}, \tag{47}$$

and by substituting ~~Eq.s~~Eqs. (10) and (12) an expression as function of the spear position is obtained

$$\tau_{\mathrm{sys}} = \frac{V_{\mathrm{p,h}} V_{\mathrm{p,k}}}{V_{\mathrm{p,b}}} \frac{1}{\eta_{\mathrm{m,h}}(\omega_{\mathrm{r}}, \Delta p_{\mathrm{h}}) \eta_{\mathrm{m,b}}(\omega_{\mathrm{b}}, \tau_{\mathrm{b}}) \eta_{\mathrm{m,k}}(\omega_{\mathrm{b}}, \Delta p_{\mathrm{k}})} \left(\frac{\rho_{\mathrm{w}}}{2} \left(\frac{Q_{\mathrm{w}}}{C_{\mathrm{d}} A_{\mathrm{nz}}(s)} \right)^2 - p_{\mathrm{k,f}} \right). \tag{48}$$

Now substituting ~~Eq.s~~Eqs. (5) and (6) in Eq. (7) results in an expression relating the water flow to the rotor speed

$$Q_{\mathrm{w}} = \frac{V_{\mathrm{p,h}} V_{\mathrm{p,k}}}{V_{\mathrm{p,b}}} \frac{\eta_{\mathrm{v,k}} \eta_{\mathrm{v,b}} \eta_{\mathrm{v,h}}}{1} \omega_{\mathrm{r}}. \tag{49}$$

Combining ~~Eq.s~~Eqs. (48) and (49), and by disregarding the water pump feed pressure $p_{\mathrm{k,f}}$ gives

$$\tau_{\mathrm{sys}} = \frac{\rho_{\mathrm{w}}}{2 C_{\mathrm{d}}^2 A_{\mathrm{nz}}^2(s)} \left(\frac{V_{\mathrm{p,h}} V_{\mathrm{p,k}}}{V_{\mathrm{p,b}}} \right)^3 \frac{\left(\eta_{\mathrm{v,h}} \eta_{\mathrm{v,b}} \eta_{\mathrm{v,k}} \right)^2}{\eta_{\mathrm{m,h}}(\omega_{\mathrm{r}}, \Delta p_{\mathrm{h}}) \eta_{\mathrm{m,b}}(\omega_{\mathrm{b}}, \tau_{\mathrm{b}}) \eta_{\mathrm{m,k}}(\omega_{\mathrm{b}}, \Delta p_{\mathrm{k}})} \omega_{\mathrm{r}}^2 = K_{\mathrm{s}} \omega_{\mathrm{r}}^2. \tag{50}$$

Rotor speed variations cause a varying flow through the spear valve, which results in a varying system pressure and thus system torque, regulating the tip-speed ratio of the rotor. The above obtained result shows that when K_{s} is constant, the tip-speed ratio can be regulated in the below-rated region by a fixed nozzle area A_{nz}. Under ideal circumstances, it is shown in (Diepeveen and Jarquin-Laguna, 2014) that ~~the nozzle area can be chosen constant to let~~ a constant nozzle area lets the rotor follow the optimal power coefficient trajectory, and is called passive torque control. This means that no active control is needed up to the near-rated operating region. For this purpose, the optimal mode gain K_{s} of the system side needs to equal that of the rotor K_{r} in the below-rated region.

However, for the passive strategy to work out, the combined drivetrain efficiency needs to be consistent in the below-rated operating region. As seen in Eq. (50), the combined efficiency term is a product of the consequent volumetric divided by the mechanical efficiencies of all components, as a function of their current operating point. To assess the consistency of the overall drivetrain efficiency, different operating strategies are examined in Sect. 4.1.1. Subsequently, a component efficiency analysis is given in Sect. 4.1.2.

4.1.1 Operational strategies

Because hydraulic components are ~~known to be~~ in general more efficient in high-load operating conditions (Trostmann, 1995), it might be advantageous for a hydraulic wind turbine drivetrain to operate the rotor at a lower tip-speed ratio. Operating at a lower tip-speed ratio results in a lower rotational rotor speed and a higher ~~system torque . The~~ torque for equal wind speeds, but at the same time decreases the rotor power coefficient C_{p}. By sacrificing rotor efficiency, the resulting higher operational pressures might ~~result in~~ lead to maximization of the total drivetrain efficiency. ~~A consequence of operating the turbine at a lower tip-speed ratio is the decreased rotor power coefficient C_{p}.~~ For these reasons, an analysis of this trade-off is divided into two cases:

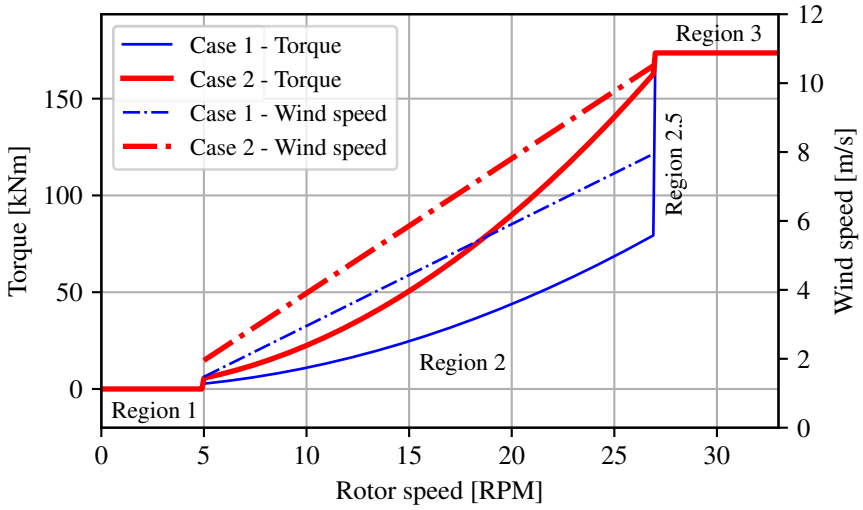

Figure 12. Torque control strategies for maintaining a fixed tip-speed ratio λ, tracking the optimal power coefficient $C_{\mathrm{p,max}}$ (case 1) and the maximum torque coefficient $C_{\tau,\mathrm{max}}$ (case 2). The dash-dotted lines show the corresponding wind speed to the distinct strategies (right y-axis), and the vertical dashed lines indicate boundaries between operating regions.

- **Case 1:** operating the rotor at its maximum power coefficient $C_{\mathrm{p,max}}$;
- **Case 2:** operation at the maximum torque coefficient $C_{\tau,\mathrm{max}}$.

Referring back to the rotor power/torque curve in Figure 6, and substituting the values for operation at $C_{\mathrm{p,max}}$ and $C_{\tau,\mathrm{max}}$ in Eq. (46), optimal mode gain values of ~~$K_{\mathrm{r,p}} = 1.00 \cdot 10^4$~~ $K_{\mathrm{r,p}} = 1.00 \cdot 10^4$ Nm (rad/s)$^{-2}$ and ~~$K_{\mathrm{r},\tau} = 2.05 \cdot 10^4$~~ $K_{\mathrm{r},\tau} = 2.05 \cdot 10^4$ Nm (rad/s)$^{-2}$ are found for cases 1 and 2, respectively. The result of evaluating the rotor torque path in the below-rated region for the two cases is presented in Figure 12. Due to the lower tip-speed ratio in case 2 , the rotor speed is lower for equal wind speeds; or a higher wind speed is required for operation at the same rotor speed resulting in a higher torque. An efficiency evaluation of the proposed operational cases, using actual component efficiency data, is given in the next section.

4.1.2 Drivetrain efficiency and stability analysis

This section presents the available component efficiency data, and evaluates steady-state drivetrain operation characteristics for the two previously introduced operating cases. The component efficiency characteristics primarily influence the steady-state response of the wind turbine, as shown in Eq. (50). To perform a fair comparison between both operating cases, the rotor efficiency is normalized with respect to case 1, resulting in a constant efficiency factor of 0.85 for operating case 2. Detailed efficiency data is available for the oil pump and motor, however, as no data for the efficiency characteristics of the water pump is available, a constant mechanical and volumetric efficiency of $\eta_{\mathrm{m,k}} = 0.83$ and $\eta_{\mathrm{m,k}} = 0.93$ are assumed, respectively. The oil pump is supplied with total efficiency data $\eta_{\mathrm{t,h}}$ as a function of the (rotor) speed ω_{r} and the supplied torque τ_{sys} (Hägglunds,

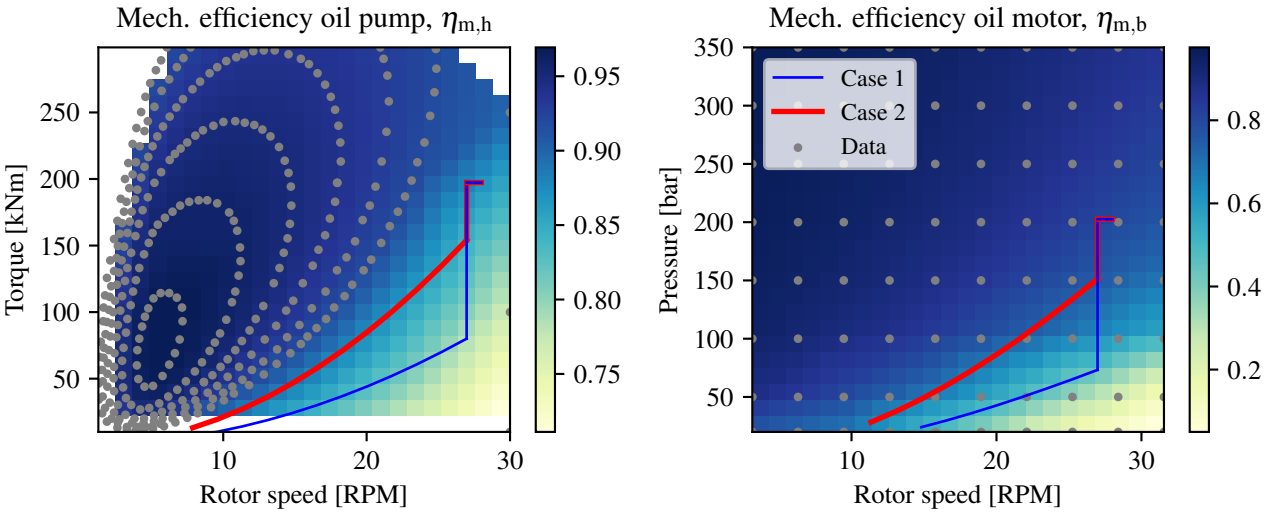

Figure 13. Mechanical efficiency mapping of the oil pump and oil motor. Manufacturer supplied data (blue dots) is evaluated using an interpolation function. Operating cases 1 and 2 are indicated by the solid blue and red lines, respectively.

2015). An expression relating the mechanical, volumetric and total efficiency is given by

$$\eta_{m,h}(\omega_r, \tau_{sys}) = \frac{\eta_{t,h}(\omega_r, \tau_{sys})}{\eta_{v,h}}, \tag{51}$$

where $\eta_{v,h}$ is taken as 0.98, and the result is presented in Figure 13 (left). The plotted data points (dots) are interpolated on a mesh grid using a regular grid linear interpolation method from the Python SciPy interpolation toolbox (Scipy.org, 2017). Operating cases 1 and 2 are indicated by the solid lines. The same procedure is performed for the data supplied with the oil motor, of which the result is presented in Figure 13 (right), where $\eta_{v,b}$ is taken as 0.98. As concluded from the efficiency curves, hydraulic components are generally more efficient in the low-speed high-torque/pressure region. It is immediately clear that for both the oil pump as well as the motor, operating the rotor at a lower tip-speed ratio (case 2) is beneficial from a component efficiency perspective.

The drivetrain efficiency analysis for both operating cases is given in Figure 14. The lack of efficiency data at lower rotor speeds in the left plot of Figure 14 (case 1) is due to unavailability of data at lower pressures. From the resulting plot it is concluded that the overall drivetrain efficiency for case 2 is higher and more consistent compared to case 1. The consistency of the total drivetrain efficiency is advantageous for control, as this ~~will enable~~ enables passive torque control to maintain a constant tip-speed ratio. As a result of this observation, the focus is henceforth shifted to the implementation of a torque control strategy tracking the maximum torque coefficient (case 2).

It should be stressed that this operational strategy is beneficial for the considered drivetrain, but can by no means be generalized for other wind turbines with hydraulic drivetrains. As the overall efficiency of hydraulic components is a product of mechanical and volumetric efficiency, a more rigorous approach would be to optimize the ideal below-rated operational

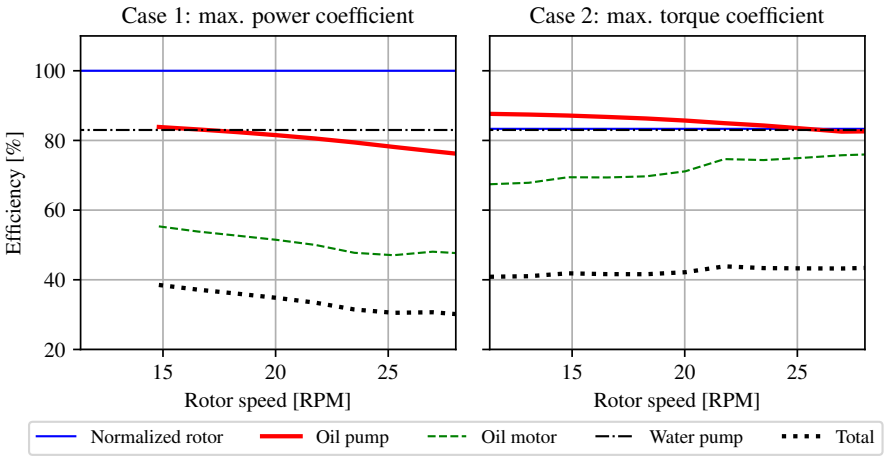

Figure 14. Comparison of the total drivetrain efficiency for operating cases 1 and 2. It is observed that the total efficiency is higher in the complete below-rated region for case 2. Also the efficiency over all rotor speeds is more consistent, enabling passive torque control using a constant nozzle area A_{nz}.

trajectory subject to all component characteristics. However, to perform a more concise analysis, only the two given trajectories are evaluated.

A stability concern for operation at the maximum torque coefficient needs to be highlighted. For stable operation, the value of k_λ needs to be negative. As shown in Figure 10, it ~~can be~~ is seen that the stability boundary is located at a tip-speed ratio of 5.9. Operation at a lower tip-speed ratio results in unstable turbine operation and deceleration of the rotor speed to standstill. However, as concluded in (Schmitz et al., 2013), hydraulic drivetrains can compensate for this theoretical instability, allowing operation at lower tip-speed ratios. Therefore, the case 2 torque control strategy ~~will be~~ is designed for the theoretical calculated minimum tip-speed ratio of 5.9, and in-field test results need to confirm the practical feasibility of the implementation.

4.2 Active near-rated torque control

A feedback hydraulic torque control is derived for near-rated operation in this section. To this end, active spear position control is employed to regulate the rotor speed. The effect on fluid resonances is analyzed, as these are possibly excited by an increased rotor speed control bandwidth. The in-field tests with corresponding control implementations are performed prior to the theoretical dynamic analysis of the drivetrain. For this reason, the control design and tunings used in-field are evaluated and possible improvements are highlighted. Sections 4.2.1 and 4.2.2 define the modeling parameters of the oil column and spear valve actuator, which is used in Sect. 4.2.3 for spear valve torque controller design.

4.2.1 Defining the hydraulic model parameters

The high-pressure oil line in the DOT500 drivetrain is considered to contain SAE30 oil, with a density of ~~$\rho_\mathrm{o} = 900$~~ $\rho_\mathrm{o} = 900$ kg m^{-3}, and an effective bulk modulus of ~~$K_{\mathrm{f,o}} = 1.5 \cdot 10^9$ Pa~~$K_{\mathrm{f,o}} = 1.5$ GPa. The hydraulic line is cylindrical with a length of ~~$L_\mathrm{l} = 50$ m~~and $L_\mathrm{l} = 50$ m, a radius of ~~$r_\mathrm{l} = 50 \cdot 10^{-3}$ m.~~ $r_\mathrm{l} = 43.3$ mm and a bulk modulus of $K_\mathrm{l} = 0.80$ GPa (Hružík et al., 2013). According to Eq. A5, the equivalent bulk modulus becomes $K_\mathrm{e} = 0.52$ GPa. The dynamic viscosity of SAE30 oil is taken at a fixed temperature of 20 °C, where it reads a value of ~~$\mu = 240 \cdot 10^{-3}$ Pa~~$\mu = 240$ mPa s. With this data the hydraulic inductance, resistance and capacitance have calculated values of ~~$I_\mathrm{H} = 5.730 \cdot 10^6$~~ $I_\mathrm{H} = 7.64 \cdot 10^6$ kg m^{-4}, ~~$R_\mathrm{H} = 4.889 \cdot 10^6$~~ $R_\mathrm{H} = 8.69 \cdot 10^6$ kg m^{-4} s^{-1} and ~~$1/C_\mathrm{H} = 3.820 \cdot 10^9$~~ $1/C_\mathrm{H} = 1.77 \cdot 10^9$ kg m^{-4} s^{-2}, respectively. Using Eq. (B4), the flow is calculated to be laminar as ~~$Re = 1177$~~ $Re = 1244$ with an oil flow at nominal rotor speed of ~~1478~~1478 l min^{-1}, and thus a correction factor $f_\mathrm{c} = 4/3$ is applied to the hydraulic inductance.

By substitution of the calculated values in Eq. (21), a visualization of the transfer function frequency response is given in Figure 15 at a range of hydraulic line lengths. In this Bode plot, it is shown that the line length has great influence on the location of the natural frequency and damping ~~ratio~~coefficient. A longer line shifts the frequency to lower values and increases the damping ~~ratio.~~ coefficient.

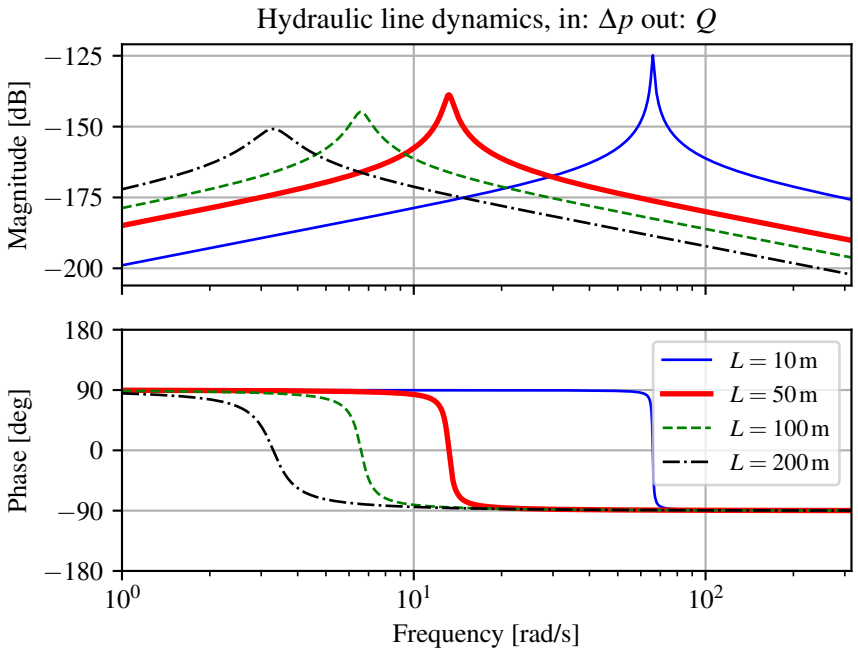

Figure 15. Bode plot of a hydraulic control volume modeled as an harmonic oscillator with pressure change Δp as input and flow Q as output. The length of the hydraulic line has great influence on the location of the natural frequency and magnitude of the damping coefficient.

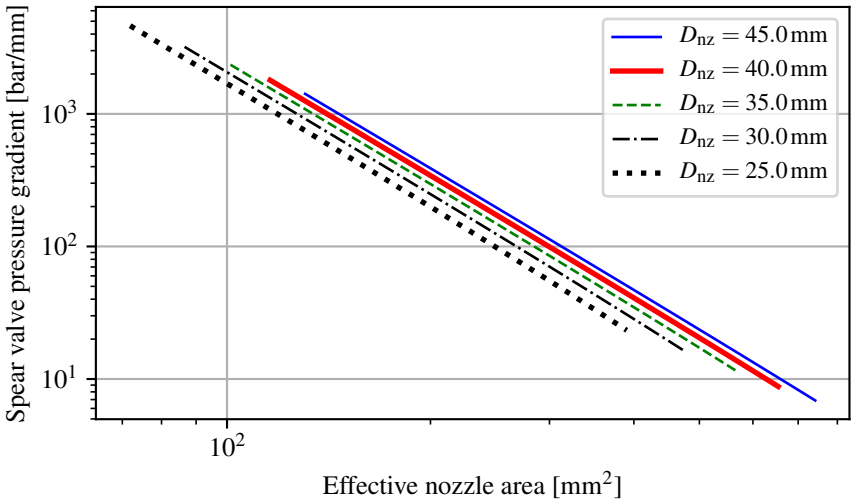

Figure 16. ~~Bode plot of a hydraulic control volume modeled as an harmonic oscillator with~~ Spear valve position pressure ~~change Δp as input and flow Q as output~~gradient, evaluated for different nozzle head diameters at a range of effective nozzle areas. The ~~length of the hydraulic line has great influence on the location of the natural frequency and magnitude of the damping ratio~~pressure sensitivity is higher for larger nozzle diameters at equal effective areas. Results are presented in a double-logarithmic plot.

4.2.2 Modeling spear valve characteristics

For determining the ~~spear valve~~ time constant t_s of the spear valve actuator model defined in Eq. (26), a Generalized pseudo-random Binary Noise (GBN) identification signal (Godfrey, 1993) is supplied to one of the spear valve actuators. From this test it is seen that the actuator has a fixed and rate-limited positioning speed of ~~$\dot{s}_{max} = 0.44$~~ $\dot{s}_{max} = 0.44$ mm s^{-1}, and shows no observable transient response. ~~The measured spear valve position is always higher or lower than the requested set point, which is an inevitable consequence of the deadband control implementation and the absence of proportional spear actuation capabilities.~~

Because of the non-linear rate-limited response, an actuator model ~~will be~~ is parameterized for the worst-case scenario. This is done by evaluating the response at maximum actuation amplitude and determining the corresponding bandwidth, such that closed-loop reference position tracking is ensured. As concluded from in-field experiments, the spear position control range in the near-rated operating region is ~~$s_{max} = 1.5$ mm. Considering excitation with a sinusoidal signal $s = s_{max} \sin(\omega_{s,max} t)$, the corresponding maximum bandwidth $\omega_{s,max}$, and thus~~ 1.5 mm, and the corresponding time-constant ~~t_s~~ for reference tracking is given by

~~$\dot{s}_{max} = \frac{1}{2} s_{max} \omega_{s,max} \cos(\omega_{s,max} t), \quad t_s = \frac{1}{\omega_{s,max}} = 1.69$ s.~~

$t_s = 1.69$ s.

The spear position relates in a non-linear fashion to the applied system torque, as a consequence of the spear valve geometry presented in Figure 8 and 9. Therefore, in Figure 16, an evaluation of the spear valve pressure gradient with respect to the spear position $k_{\mathrm{s,s}}$ is given~~in Figure 16~~. This is done for distinct nozzle head diameters at a range of effective nozzle areas. It is shown that the spear pressure gradient with respect to the position is higher for larger nozzle head diameters at equal effective areas. ~~Spear valve position pressure gradient, evaluated for different nozzle head diameters at a range of effective nozzle areas. The pressure sensitivity is higher for larger nozzle diameters at equal effective areas. Results are presented in a double-logarithmic plot.~~

4.2.3 Torque control design and evaluation

The active spear valve torque control strategy employed during the in-field tests is now evaluated. A fixed-gain controller was implemented for rotor speed control in the near-rated region. As the goal is to make a fair comparison and evaluation of the in-field control design, the same PI controller is used in this analysis. ~~Bode plot of open-loop transfer including controller from spear valve position reference to the rotor speed.~~ **without** ~~spear valve pressure feedback gain $k_{\mathrm{s,Q_w}}$.~~

The dynamic drivetrain model presented in Sect. 3.2 is further analyzed. The linear state-space system in Eq. (44) is evaluated at different operating points in the near-rated region. The operating point is chosen at a rotor speed of ~~$\omega_{\mathrm{r,s}} = 27$~~$\omega_{\mathrm{r,s}} = 27$ RPM, which results in a water pump discharge flow of ~~$\bar{Q}_{\mathrm{w}} = 2965$~~$\bar{Q}_{\mathrm{w}} = 2965$ l min^{-1}, taking into account the volumetric losses. For the entire near-rated region, a range of wind speeds and corresponding model parameters are computed and are listed in Table 2. An analysis is performed on the Single-Input Single-Output (SISO) open-loop transfer system with the speed error e_{s} as input and rotor speed as output, including the spear valve PI torque controller used during field tests. The gains of the PI controller were ~~$K_{\mathrm{p}} = 3.8 \cdot 10^{-3}$~~$K_{\mathrm{p}} = 3.8 \cdot 10^{-3}$ m (rad/s)$^{-1}$, and ~~$K_{\mathrm{i}} = 6.6845 \cdot 10^{-4}$~~$K_{\mathrm{i}} = 6.6845 \cdot 10^{-4}$ m rad^{-1}.

By inspection of the state A-matrix, various preliminary remarks can be made regarding system stability and drivetrain damping. First it is seen that for the $(2,\ 2)$-element, the hydraulic resistance R_{H} influences the intrinsic speed feedback gain $k^*_{Q_{\mathrm{in}}}$. It was concluded in Sect. 4.1.2 that the rotor operation is stable for negative values of $k_{\omega_{\mathrm{r}}}$ and thus $k^*_{Q_{\mathrm{in}}}$. Thus, the higher the hydraulic resistance, the longer the $(2,\ 2)$-element stays negative for decreasing tip-speed ratios, resulting in increased operational stability. This effect has been observed earlier in (Schmitz et al., 2012, 2013), where it was shown that turbines with a hydraulic drivetrain are able to attain lower tip-speed ratios. This is in accordance with ~~Eq.s~~Eqs. (B7) and (B8), where it is shown that the resistance term only influences the damping. Furthermore, the spear valve pressure feedback gain $k_{\mathrm{s,Q_w}}$ provides additional system torque when the rotor has a speed increase or overshoot, resulting in additional damping to the $(3,\ 3)$-element in the state matrix.

During analysis, an important result is noticed and is shown by discarding and including the spear valve pressure feedback gain $k_{\mathrm{s,Q_w}}$ in the linearized state-space system. The open-loop Bode plot of the system excluding the term is presented in Figure 17, and including the term in Figure 18. It is noted that the damping term completely damps the hydraulic resonance peak in the oil column as a result of the intrinsic flow-pressure feedback effect. At the same time, the attainable bandwidth of the hydraulic torque control implementation is limited. This bandwidth limiting effect becomes more severe by applying

Table 2. Parameters for linearization of the model in the near-rated operating region.

Description	Symbol	Value	Unit
Wind speed	$\bar{U}$	$10.6 - 11.8$	m s^{-1}
Rotor speed set point	$\bar{\omega}_\mathrm{r}$	27.0	RPM
Water flow	$\bar{Q}_\mathrm{w}$	2965	l min^{-1}
Water pressure	$\bar{p}_\mathrm{w,l}$	$51.4 - 62.4$	bar
Oil flow	$\bar{Q}_\mathrm{o}$	1354	l min^{-1}
Oil pressure	$\Delta\bar{p}_\mathrm{h}$	$166 - 201$	bar
Rotor torque	$\bar{\tau}_\mathrm{r}$	$163.8 - 198.7$	kNm
Rotor inertia	J_r	$6.6 \cdot 10^5$	kg m^2
Nozzle diameter	D_nz	38	mm
Spear coning angle	α	50	deg
Number of spear valves	N_s	2	-
Discharge coefficient	C_d	1.0	-
Effective nozzle area	A_nz	$486.9 - 442$	mm^2
Spear position	$\bar{s}$	$4.64 - 4.18$	mm
Density of air	ρ_a	1.225	kg m^{-3}
Density of oil	ρ_o	900	kg m^{-3}
Density of water	ρ_w	998	kg m^{-3}
Component mechanical efficiency	$\eta_\mathrm{m,x}$	0.85	-
Component volumetric efficiency	$\eta_\mathrm{v,x}$	0.95	-
Hydraulic line radius	r_l	~~50.0~~ 43.3	mm
Hydraulic line length	L_l	50.0	m
Hydraulic line volume	V_H	~~392.6~~ 295	l
Hydraulic induction, oil	L_H	~~$5.730 \cdot 10^6$~~ $7.64 \cdot 10^6$	kg m^{-4}
Hydraulic resistance, oil	R_H	~~$4.889 \cdot 10^6$~~ $8.69 \cdot 10^6$	kg m^{-4}s^{-1}
~~Effective~~ Equivalent bulk modulus, oil and line	~~K_f~~ K_e	~~1.5~~ 0.52	GPa
Dynamic viscosity, oil	μ_o	0.240	Pa s
Spear valve actuator time constant	t_s	1.69	s
Pitch actuator time constant	t_s	0.5	s

longer line lengths and thus larger volumes in the discharge line, as it increases the hydraulic induction. Fortunately, various solutions are possible to mitigate this effect and are discussed next.

The effect of increasing different model parameters is depicted in Figure 18. In the DOT500 set-up an intermediate oil circuit is used, which ~~will be~~ is omitted in the ideal DOT concept. Seawater has a higher effective bulk modulus compared to oil and

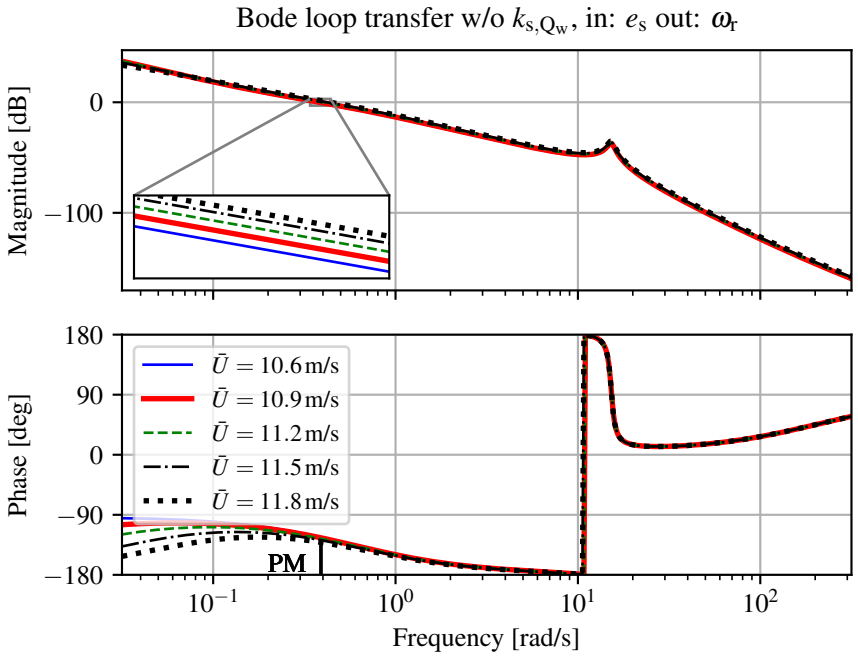

Figure 17. Bode plot of open-loop transfer including controller from spear valve position reference to the rotor speed, **without** spear valve pressure feedback gain k_{s,Q_w}. The phase margin (PM) at magnitude cross-over is indicated.

this has a positive effect on the maximum attainable torque control bandwidth for equal line lengths. Moreover, a faster spear valve actuator has a positive influence on the attainable control bandwidth.

From both figures it is also observed that the system dynamics change according to the operating point. At higher wind speeds, the magnitude response results is higher. The effect was earlier seen in Figure 16, where the pressure gradient with respect to the spear valve position is higher for smaller effective nozzle areas. It is concluded that the sizing of the nozzle diameter is a trade-off between the minimal achievable pressure and its controllability with respect to the resolution of the spear positioning and actuation speed.

~~Closed-loop step responses throughout the near-rated region (for different wind speeds) are shown in Figure 19. It is seen that the controller stabilizes the system, and the control bandwidth increases for higher wind speeds.~~ The loop-shaped frequency responses attain a minimum and maximum bandwidth of 0.35 and ~~0.43~~0.43 rad s^{-1} with phase margins ~~of 55 and 40~~ (PM) of 64 and 58 deg, respectively. For later control designs a more consistent control bandwidth can be attained by gain-scheduling the controller gains on a measurement of the water pressure or spear position. Closed-loop step responses throughout the near-rated region (for different wind speeds) are shown in Figure 19. It is seen that the controller stabilizes the system, and the control bandwidth increases for higher wind speeds.

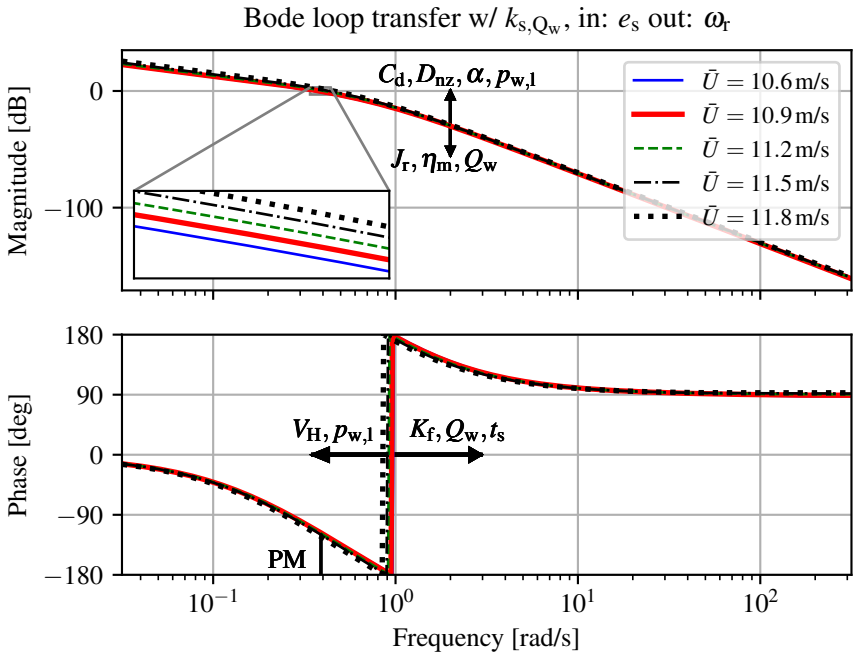

Figure 18. Bode plot of the plant for transfer from spear valve position reference to the rotor speed, **with** spear valve pressure feedback gain k_{s,Q_w}. The effect of increasing important model parameters on the frequency response is indicated, together with the phase margin (PM) at the magnitude cross-over frequency.

5 Implementation of control strategy and in-field results

This section covers the implementation and evaluation of the derived control strategies on the real-world in-field DOT500 turbine. In accordance with the previous section, a distinction is made between passive and active regulation, for below- and near-rated wind turbine control, respectively. To illustrate the overall control strategy from in-field gathered test data, operational visualizations are given in Sect. 5.1. Evaluation of the effectiveness of the passive below-rated and active near-rated torque control strategy is presented in Sect. 5.2.

5.1 Turbine performance characteristics and control strategy

To illustrate the overall control strategy, three-dimensional rotor torque and rotor speed plots are shown as a function of spear position and wind speed in Figure 20. By fixing the valve position at a range of positions, making sure that sufficient data is collected throughout all wind speeds and binning the data accordingly, a steady-state drivetrain performance mapping is derived. Both figures show the data binned in predefined spear valve positions and wind speeds. This is done on a normalized scale, where ~~0~~0 % is the maximum spear position (larger nozzle area), and ~~100~~100 % the minimum spear position (smaller nozzle area). The absolute difference between the minimum and maximum spear position is ~~1.5~~1.5 mm. The spear position is

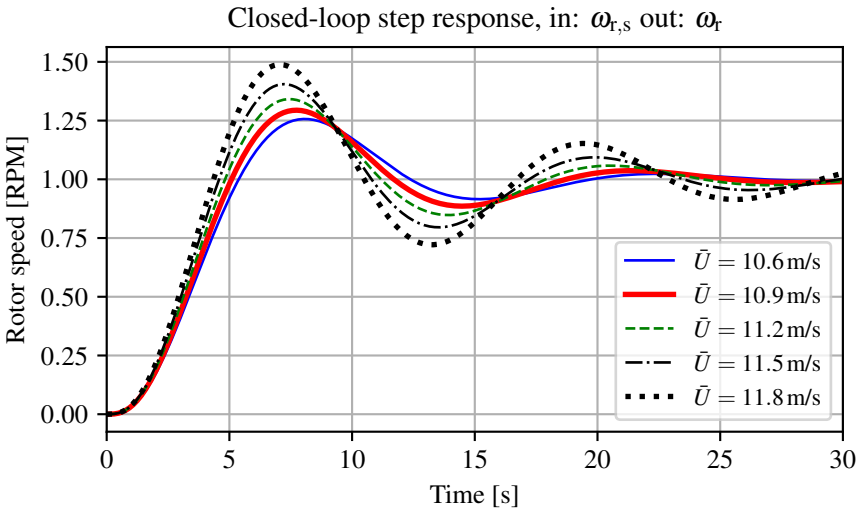

Figure 19. Closed-loop step responses of the spear valve torque control implementation. It is shown that the feedback loop is stabilized, but that the dynamics vary with increasing wind speeds. A control implementation that takes care of the varying spear valve position pressure gradient would load to a more consistent response.

the only control input in the below-rated region, and is independent from other system variables. During data collection, the pitch system regulates the rotor speed up to its nominal set point value when an overspeed occurs.

In both figures the control strategy is indicated by colored lines. For below-rated operation (red), the spear valve position is kept constant: flow fluctuations influence the water discharge pressure and thus the system torque. In near-rated conditions (blue), the spear position is actively controlled by a PI-controller. Under conditions of a constant regulated water flow corresponding to ~~$\omega_{r,s} = 27$~~ $\omega_{r,s} = 27$ RPM, the controller continuously adjusts the spear position and thus water discharge pressure to regulate the rotor speed. Once the turbine reaches its nominal power output, the rotor limits wind energy power capture using gain-scheduled PI pitch control (green), maintaining the rotor speed at ~~$\omega_{r,\beta} = 28$ RPM.~~ $\omega_{r,\beta} = 28$ RPM.

5.2 Evaluation of the control strategy

Previously, in Sect. 4.1, drivetrain characteristics are deduced from prior component information throughout the wind turbine operating region. Characteristic data from the rotor, the oil pump and the oil motor is evaluated to come up with a hydraulic torque control strategy. Due to the predicted consistent mechanical efficiency of the hydraulic drivetrain, the nozzle area can be fixed and no active torque control is needed in the below-rated region. This results from the rotor speed being proportional to water flow, and relates to system torque according to Eq. (50). From the analysis it is also concluded that operating at a lower tip-speed ratio, results in a higher and more consistent overall efficiency for this particular drivetrain.

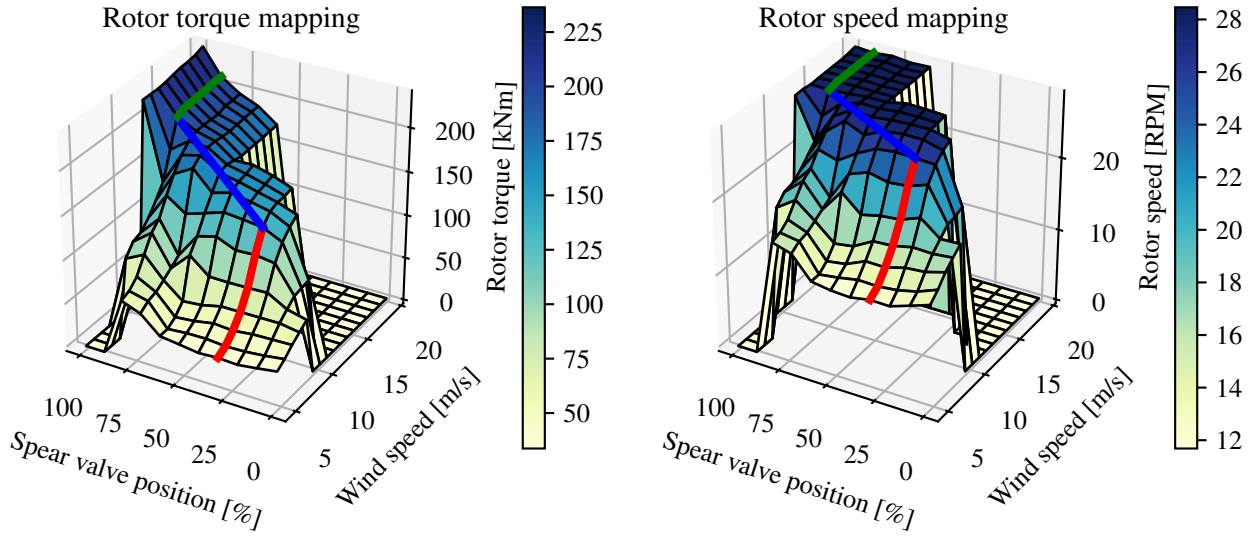

Figure 20. Steady-state rotor torque and speed at predefined spear valve positions (nozzle areas) and wind speed conditions. The red line indicates the operation strategy at fixed spear valve position in the below-rated region, whereas the blue trajectory indicates active spear valve position control towards rated conditions. The effect of blade pitching is indicated in green.

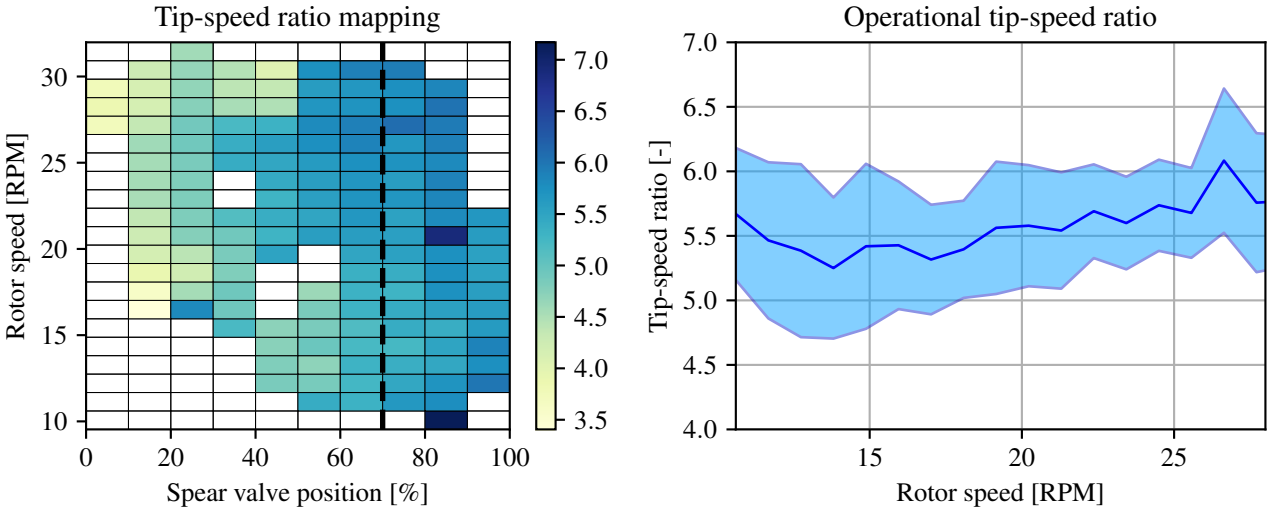

Figure 21. Tip-speed ratio mapping as function of spear valve position and rotor speed (left). The dashed line indicates the fixed spear position selected for below-rated passive torque control. The right plot shows the corresponding evaluation of the tip-speed ratios along this path with 1σ standard deviation bands.

As concluded in Sect. 4.1.2, stable turbine operation is attained when the rotor operates at a tip-speed ratio such that k_λ is negative, and Figure 10 shows that the predicted stability boundary is located at a tip-speed ratio of $\lambda = 5.9$. Using the obtained data from in-field tests, a mapping of the attained tip-speed ratios as function of the spear valve position and rotor speed is given in Figure 21. An anemometer on the nacelle and behind the rotor measures the wind speed. As turbine wind speed measurements are generally considered less reliable (Østergaard et al., 2007) and the effect of induction is not included in this analysis, the obtained results serve as an indication of the turbine behavior. The dashed line indicates the fixed spear position of ~~70~~70 %, and is chosen as the position for passive torque control in the below-rated region. The attained tip-speed ratio averages are presented in the left plot, and the right plot shows a two-dimensional visualization of the data indicated by the dashed line, including one standard deviation. Closing the spear valve further for operation at an even lower tip-speed ratio and higher water pressures, resulted in a slowly decreasing rotor speed and thus unstable operation. ~~Tip-speed ratio mapping as function of spear valve position and rotor speed (left). The dashed line indicates the fixed spear position selected for below-rated passive torque control. The right plot shows the corresponding evaluation of the tip-speed ratios along this path with 1σ standard deviation bands.~~

In Figure 21, it is shown that the calculated tip-speed ratio is regulated around a mean of 5.5 for below-rated conditions. Although the attained value is lower than the theoretical calculated minimum tip-speed ratio of 5.9, stable turbine operation is attained during in-field tests. A plausible explanation is that the damping characteristics of hydraulic components compensate for instability as predicted in Sect. 4.2.3.

Figure 22 shows reaction torque measurements by the load-pins in the suspension of the oil pump to estimate the attained rotor torque during below-rated operation. From the tip-speed ratio heat map and the rotor torque measurements it is concluded that the case 2 (maximum rotor torque coefficient) strategy works out on the actual turbine, and the passive strategy regulates the torque close to the desired predefined path. However, as ~~can be~~ seen in both figures for lower rotor speeds, the tip-speed ratio attains lower values and the rotor torque increases. An explanation for this effect is the decreased mechanical water pump efficiency, of which, as earlier stated, the efficiciency characteristics are unknown. An analysis of the water pump efficiency is performed using measurement data and show non-constant mechanical efficiency characteristics: the efficiency drops rapidly when the rotor speeds is below ~~15~~15 RPM.

Finally, the active spear valve torque control strategy is evaluated. The aim is to regulate the rotor speed to a constant reference speed in the near-rated operating region. In-field test results are given in Figure 23, ~~and all~~ where the environmental conditions were such that the turbine operated around the near-rated region. All values are normalized for convenient presentation. It is shown that active spear valve control combined with pitch control regulates the wind turbine for (near-)rated conditions in a decentralized way. Small excursions to the below-rated region are observed when the spear valve position saturates at is minimal normalized value. The spear position tracks the control signal reference, and shows that the strategy has sufficient bandwidth to act as a substitute to conventional torque control.

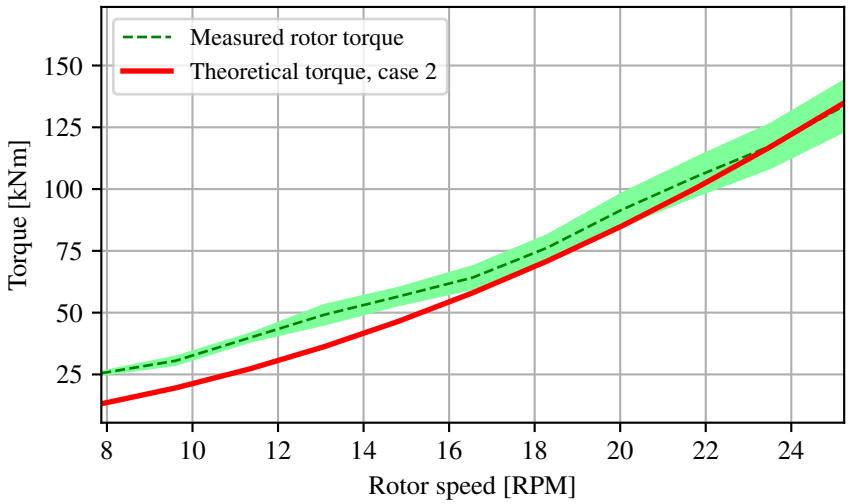

Figure 22. Evaluation of the passive torque control strategy, by comparison of the theoretical torque for case 2 to the torque measured by load-pins in the oil pump suspension. For higher speeds, the passive torque control strategy succeeds in near-ideal tracking of the desired case 2 path. At lower rotor speeds, the torque is higher than the aimed theoretical line, resulting from the lower combined drivetrain efficiency in this operating region.

6 Conclusions

This paper presents the control design for the intermediate DOT500 hydraulic wind turbine. This turbine with a ~~500~~500 kW hydraulic drivetrain is deployed in-field and served as proof of concept. The drivetrain included a hydraulic transmission in the form of an oil circuit, as at the time of writing a low-speed high-torque seawater pump was not commercially available, and is being developed by DOT.

First it is concluded that for the employed drivetrain, operating at maximum rotor torque, instead of maximum rotor power, is beneficial for drivetrain efficiency maximization. This results not only in an increased overall efficiency, but comes with an additional advantage of the ~~mechanical~~ efficiency characteristics being consistent for the ~~drivetrain. It is concluded that for a successful application of below-rated passive torque control~~ considered drivetrain. From a control perspective, a consistent overall drivetrain efficiency is required for successful application of the below-rated passive torque control strategy. Another benefit of the hydraulic drivetrain is the added damping, enabling operation at lower tip-speed ratios. It is shown using in-field measurement data that the passive strategy succeeds in tracking the torque path corresponding to maximum rotor torque for a large envelope in the below-rated region. For a smaller portion, the combined drivetrain mechanical efficiency drops, which results in deviation from the desired trajectory.

Secondly, a drivetrain model including the oil dynamics is derived for spear valve control design in the near-rated region. It is shown that by including a spear valve as a control input, the hydraulic resonance is damped by the flow induced spear

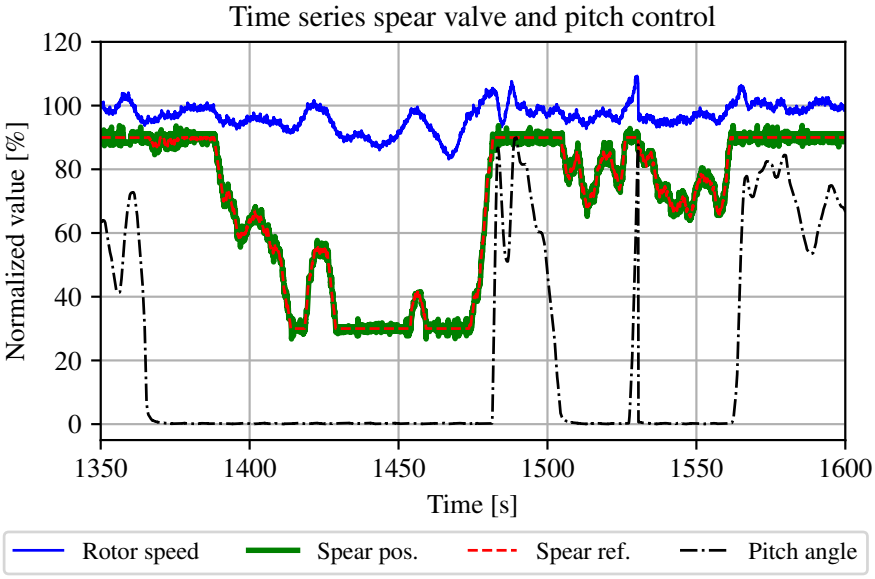

Figure 23. A time-series showing the hydraulic control strategy for the DOT500 turbine. The spear valve position actively regulates the rotor speed as a substitute to conventional turbine torque control. In the above-rated region, pitch control is employed to keep the rotor at it nominal speed. All signals in this plot are normalized.

valve pressure feedback. This intrinsic pressure feedback effect also limits the attainable torque control bandwidth. However, this limiting effect can be coped with by using a stiffer fluid, a decreased hydraulic line volume or a faster spear valve actuator. The sizing of the nozzle head diameter influences the pressure sensitivity with respect to the spear position, and affects the attainable control bandwidth by spear valve actuation speed constraints and positioning accuracy. In-field test results show the practical feasibility of the strategy including spear valve and pitch control inputs to actively regulate the wind turbine in the (near-)rated operating region. Future control designs will be improved by including a control implementation taking into account the varying spear valve pressure gradient. This will result in a higher and more consistent system response.

The ideal DOT concept discards the oil circuit and only uses water hydraulics with an internally developed seawater pump. As a result, the control design process is simplified and the overall drivetrain efficiency ~~will~~ should be greatly improved. Future research will focus on the design of a centralized control implementation for DOT wind turbines acting in a hydraulic network.

Appendix A: Definition of hydraulic induction, resistance and capacitance for Sect. 3.2.1

Hydraulic induction: the hydraulic induction L_H resembles the ease of acceleration of a fluid volume and is related to the fluid inertia I_f by

$$L_\mathrm{H} = f_\mathrm{c} I_\mathrm{f} = f_\mathrm{c} \frac{\rho L_\mathrm{l}}{A}, \tag{A1}$$

with the assumption that the flow speed profile is radially uniform (Akers et al., 2006). For this reason, a distinction should be made between laminar and turbulent flows in circular lines: the induction of a laminar flow is generally corrected by a factor $f_\mathrm{c} = 4/3$, whereas a turbulent flow does not need correction with respect to the fluid inertia I_f (Bansal, 1989).

Hydraulic resistance: the hydraulic resistance dissipates energy from a flow in the form of a pressure decrease over a hydraulic element. In most cases, hydraulic resistances are taken as an advantage by means of control valves. For example, by adjusting a valve set point, one adjusts the resistance to a desired value. Mathematically, the hydraulic resistance relates the flow rate to the corresponding pressure drop

$$\Delta p_\mathrm{R} = Q R_\mathrm{H}, \tag{A2}$$

analogous to an electrical circuit where the voltage over a resistive element equals the current times the resistance. The hydraulic resistance for a hydraulic line with a circular cross section and a laminar flow is

$$R_\mathrm{H,l} = \frac{8 \mu L_\mathrm{l}}{\pi r_\mathrm{l}^4}, \tag{A3}$$

which is a constant term independent of the flow rate. For a turbulent fluid flow, the computation of the resistance is more involved and results in a quantity that is dependent on the flow rate and effective pipe roughness. For simulation purposes this would require re-evaluation of the resistance in each time step, or for each operating point during linear analysis. Such a Non-Linear Time-Variant (NLTV) system is employed in (Buhagiar et al., 2016), updating the resistive terms in each iteration for a hydraulic variable-displacement drivetrain with seawater under turbulent conditions.

Hydraulic capacitance: due to fluid compressibility and line elasticity, the amount of fluid can change as a result of pressure changes in a control volume. The effective bulk modulus K_f of a fluid is defined by the pressure increase to the relative decrease of the volume

$$dp = K_\mathrm{f} \frac{dV}{V_\mathrm{H}}, \qquad K_\mathrm{f} = V_\mathrm{H} \frac{dp}{dV}. \tag{A4}$$

The equivalent bulk modulus (Merritt, 1967) of a compressible fluid without vapor or entrapped air, in a flexible line with bulk modulus K_l is defined as

$$K_\mathrm{e} = \left(\frac{1}{K_\mathrm{f}} + \frac{1}{K_\mathrm{l}} \right)^{-1}. \tag{A5}$$

Subsequently, the pressure change with respect to time is

$$\dot{p} = \frac{dp}{dt} = K_\mathrm{fe} \frac{1}{V_\mathrm{H}} \frac{dV}{dt} = \frac{K_\mathrm{f}}{V_\mathrm{H}} \frac{K_\mathrm{e}}{V_\mathrm{H}} Q = \frac{1}{C_\mathrm{H}} Q, \tag{A6}$$

and thus the hydraulic capacitance C_{H} is directly proportional to the volume amount and gives the pressure change according to a net flow variation into a control volume.

Appendix B: Model derivation of a hydraulic control volume for Sect. 3.2.1

For modeling a the dynamics of a volume in a hydraulic line, analogies between mechanical and hydraulic systems are employed for modeling convenience. First, the differential equation for a standard mass-damper-spring system driven by an external force F is given by

$$F = m\ddot{x} + c\dot{x} + kx. \tag{B1}$$

For conversion to a hydraulic equivalent expression, the driving mechanical force is substituted by $F = \Delta p A$, the control volume mass is taken as $m = \rho V_\mathrm{H} = \rho A L_\mathrm{l}$, and the fluid inflow velocity defined as $\dot{x} = Q/A$. By rearranging terms, one obtains

$$\Delta p = \frac{\rho L_\mathrm{l}}{A}\dot{Q} + \frac{c}{A^2}Q + \frac{k}{A^2}\int Q dt, \tag{B2}$$

which is further simplified into

$$\Delta p = L_\mathrm{H}\dot{Q} + R_\mathrm{H}Q + \frac{1}{C_\mathrm{H}}\int Q dt, \tag{B3}$$

where L_H, R_H and C_H are the hydraulic induction, resistance and capacitance (Esposito, 1969), respectively, and are defined in Appendix A. The former two of these three quantities depend on the flow Reynolds number, which shows whether the inertial or viscosity terms are dominant in the Navier-Stokes equations (Merritt, 1967). The Reynolds number is defined as

$$Re = \frac{D_\mathrm{l} v \rho}{\mu}, \tag{B4}$$

where $D_\mathrm{l} = 2r_\mathrm{l}$ is the line diameter, and μ the fluid dynamic viscosity. For Reynolds numbers larger than 4000 the flow is considered as turbulent and the inertial terms are dominant, whereas for values smaller than 2300 the viscosity terms are deemed dominant.

For evaluation of the natural frequency ω_n and damping coefficient ζ for the considered system, the characteristic equation by neglecting the external excitation force ($\Delta p = 0$) is defined as

$$0 = \dot{Q} + \frac{R_\mathrm{H}}{L_\mathrm{H}}Q + \frac{1}{C_\mathrm{H}L_\mathrm{H}}\int Q dt \tag{B5}$$

$$= \dot{Q} + 2\zeta\omega_\mathrm{n}Q + \omega_\mathrm{n}^2\int Q dt. \tag{B6}$$

Evaluating the quantities ω_n and ζ, results in

$$\omega_\mathrm{n} = \sqrt{\frac{1}{C_\mathrm{H}L_\mathrm{H}}}, \tag{B7}$$

$$\zeta_\mathrm{p} = \frac{R_\mathrm{H}}{2}\sqrt{\frac{C_\mathrm{H}}{L_\mathrm{H}}}. \tag{B8}$$

The inverse result of Eq. (B3) is obtained (Murrenhoff, 2012), with flow Q as the external excitation and Δp as output

$$Q = C_{\mathrm{H}} \Delta \dot{p} + \frac{1}{R_{\mathrm{H}}} \Delta p + \frac{1}{L_{\mathrm{H}}} \int \Delta p dt. \tag{B9}$$

Now by evaluating the characteristic equation

$$0 = C_{\mathrm{H}} \Delta \dot{p} + \frac{1}{R_{\mathrm{H}}} \Delta p + \frac{1}{L_{\mathrm{H}}} \int \Delta p dt \tag{B10}$$

$$= \Delta \dot{p} + \frac{1}{R_{\mathrm{H}} C_{\mathrm{H}}} \Delta p + \frac{1}{L_{\mathrm{H}} C_{\mathrm{H}}} \int \Delta p dt, \tag{B11}$$

and using Eq. (B6), it is seen that the natural frequency remains unchanged with the result obtained in Eq. (B7), but the definition of the damping coefficient changes

$$\zeta_{\mathrm{Q}} = \frac{1}{2R_{\mathrm{H}}} \sqrt{\frac{L_{\mathrm{H}}}{C_{\mathrm{H}}}}. \tag{B12}$$

Finally, the differential equation defined by Eq. (B3) is expressed as a transfer function in

$$G_{\mathrm{Q/\Delta p}}(s) = \frac{1/L_{\mathrm{H}}}{s + (R_{\mathrm{H}}/L_{\mathrm{H}}) + 1/(C_{\mathrm{H}} L_{\mathrm{H}} s)} \tag{B13}$$

$$= \frac{s/L_{\mathrm{H}}}{s^2 + (R_{\mathrm{H}}/L_{\mathrm{H}}) s + 1/(C_{\mathrm{H}} L_{\mathrm{H}})}, \tag{B14}$$

and the same is done for Eq. (B9)

$$G_{\mathrm{\Delta p/Q}}(s) = \frac{1/C_{\mathrm{H}}}{s + 1/(R_{\mathrm{H}} C_{\mathrm{H}}) + 1/(C_{\mathrm{H}} L_{\mathrm{H}} s)} \tag{B15}$$

$$= \frac{s/C_{\mathrm{H}}}{s^2 + 1/(R_{\mathrm{H}} C_{\mathrm{H}}) s + 1/(C_{\mathrm{H}} L_{\mathrm{H}})}. \tag{B16}$$

Competing interests. The authors declare that they have no conflict of interest.

Acknowledgements. The research presented in this paper was part of the DOT500 ONT project, which was conducted by DOT in collaboration with Delft Univeristy of Technology and executed with funding received from the *Ministerie van Economische zaken via TKI Wind op Zee, Topsector Energie.*

References

Akers, A., Gassman, M., and Smith, R.: Hydraulic power system analysis, CRC press, 2006.

Al'tshul', A. D. and Margolin, M. S.: Effect of vortices on the discharge coefficient for flow of a liquid through an orifice, Hydrotechnical Construction, 2, 507–510, 1968.

Artemis Intelligent Power: http://www.artemisip.com/sectors/wind/, 2018.

Bansal, R.: A Text Book of Fluid Mechanics and Hydraulic Machines: In MKS and SI Units, Laxmi publications, 1989.

Bianchi, F. D., De Battista, H., and Mantz, R. J.: Wind turbine control systems: principles, modelling and gain scheduling design, Springer Science & Business Media, 2006.

Bosch-Rexroth: Axial Piston Variable Motor A6VM - Sales information/Data sheet, Tech. rep., Bosch-Rexroth, 2012.

Bossanyi, E. A.: The design of closed loop controllers for wind turbines, Wind Energy, 3, 149–163, 2000.

Bragg, S.: Effect of compressibility on the discharge coefficient of orifices and convergent nozzles, Journal of Mechanical Engineering Science, 2, 35–44, 1960.

Brekke, H.: Hydraulic turbines: design, erection and operation, Norwegian University of Science and Technology (NTNU), 2001.

Buhagiar, D. and Sant, T.: Steady-state analysis of a conceptual offshore wind turbine driven electricity and thermocline energy extraction plant, Renewable Energy, 68, 853–867, 2014.

Buhagiar, D., Sant, T., and Bugeja, M.: A comparison of two pressure control concepts for hydraulic offshore wind turbines, Journal of Dynamic Systems, Measurement, and Control, 138, 081 007, 2016.

Burton, T., Jenkins, N., Sharpe, D., and Bossanyi, E.: Wind energy handbook, John Wiley & Sons, 2011.

Cabrera, E., Espert, V., and Martínez, F.: Hydraulic Machinery and Cavitation: Proceedings of the XVIII IAHR Symposium on Hydraulic Machinery and Cavitation, Springer, 2015.

Chapple, P., Dahlhaug, O., and Haarberg, P.: Turbine driven electric power production system and a method for control thereof, 2011.

Diepeveen, N.: On the application of fluid power transmission in offshore wind turbines, Ph.D. thesis, Delft University of Technology, 2013.

Diepeveen, N. and Jarquin-Laguna, A.: Wind tunnel experiments to prove a hydraulic passive torque control concept for variable speed wind turbines, in: Journal of Physics: Conference Series, vol. 555, IOP Publishing, 2014.

Diepeveen, N., Mulders, S., and Tempel, J. v. d.: Field tests of the DOT500 prototype hydraulic wind turbine, International Fluid Conference 2018, 2018a.

Diepeveen, N., Mulders, S., and van der Tempel, J.: Field tests of the DOT500 prototype hydraulic wind turbine, in: 11th International Fluid Power Conference, pp. 530–537, Aachen, 2018b.

Esposito, A.: A simplified method for analyzing hydraulic circuits by analogy, Machine Design, 41, 173, 1969.

EWEA: The economics of wind energy, EWEA, 2009.

Fingersh, L., Hand, M., and Laxson, A.: Wind turbine design cost and scaling model, Tech. rep., National Renewable Energy Lab.(NREL), Golden, CO (United States), 2006.

Godfrey, K.: Perturbation signals for system identification, Prentice Hall International (UK) Ltd., 1993.

Hägglunds: Compact CB - Product Manual, 2015.

Hružík, L., Vašina, M., and Bureček, A.: Evaluation of bulk modulus of oil system with hydraulic line, in: EPJ Web of Conferences, vol. 45, p. 01041, EDP Sciences, 2013.

Jager, S.: Control Design and Data-Driven Parameter Optimization for the DOT500 Hydraulic Wind Turbine, Master thesis, Delft University of Technology, 2017.

Jarquin Laguna, A.: Centralized electricity generation in offshore wind farms using hydraulic networks, Ph.D. thesis, Delft University of Technology, 2017.

Jonkman, J., Butterfield, S., Musial, W., and Scott, G.: Definition of a 5-MW reference wind turbine for offshore system development, Tech. rep., National Renewable Energy Lab.(NREL), Golden, CO (United States), 2009.

KAMAT: Quintuplex Plunger Pump K80000-5G, Website, https://www.kamat.de/en/plunger-pumps/k-80000-5g.html, 2017.

Kempenaar, A.: Small Scale Fluid Power Transmission for the Delft Offshore Turbine, Master's thesis, TU Delft, 2012.

Kotzalas, M. N. and Doll, G. L.: Tribological advancements for reliable wind turbine performance, Philosophical Transactions of the Royal Society of London A: Mathematical, Physical and Engineering Sciences, 368, 4829–4850, 2010.

Merritt, H. E.: Hydraulic control systems, John Wiley & Sons, 1967.

Mulders, S., Diepeveen, N., and van Wingerden, J.-W.: Control design and validation for the hydraulic DOT500 wind turbine, in: 11th International Fluid Power Conference, pp. 200–209, Aachen, 2018a.

Mulders, S. P., Diepeveen, N. F. B., and van Wingerden, J.-W.: Data set: Control design, implementation and evaluation for an in-field 500 kW wind turbine with a fixed-displacement hydraulic drivetrain, https://doi.org/10.5281/zenodo.1250459, https://doi.org/10.5281/zenodo.1250459, 2018b.

Muller, H., Poller, M., Basteck, A., Tilscher, M., and Pfister, J.: Grid compatibility of variable speed wind turbines with directly coupled synchronous generator and hydro-dynamically controlled gearbox, in: Sixth International Workshop on Large-Scale Integration of Wind Power and Transmission Networks for Offshore Wind Farms, pp. 307–315, 2006.

Murrenhoff, H.: Grundlagen der Fluidtechnik: Teil 1: Hydraulik, Shaker, 2012.

Nijssen, J., Diepeveen, N., and Kempenaar, A.: Development of an interface between a plunger and an eccentric running track for a low-speed seawater pump, International Fluid Conference 2018, 2018.

Østergaard, K. Z., Brath, P., and Stoustrup, J.: Estimation of effective wind speed, in: Journal of Physics: Conference Series, vol. 75, IOP Publishing, 2007.

Pedersen, N. H., Johansen, P., and Andersen, T. O.: Optimal control of a wind turbine with digital fluid power transmission, Nonlinear Dynamics, pp. 1–17, 2017.

Piña Rodriguez, I.: Hydraulic drivetrains for wind turbines: Radial piston digital machines, Master's thesis, Delft University of Technology, 2012.

Ragheb, A. and Ragheb, M.: Wind turbine gearbox technologies, in: Nuclear & Renewable Energy Conference (INREC), 2010 1st International, pp. 1–8, IEEE, 2010.

Rampen, W. et al.: Gearless transmissions of large wind turbines-the history and future of hydraulic drives, Artemis IP Ltd., Midlothian, UK, 2006.

Rodriguez, A. G., Rodríguez, A. G., and Payán, M. B.: Estimating wind turbines mechanical constants, in: Proc. Int. Conf. Renewable Energies and Power Quality (ICREPQ'07), pp. 27–30, 2007.

Rybak, S.: Description of the 3 MW SWT-3 wind turbine at San Gorgonio Pass California, in: Fifth Bien. Wind Energy Conference and Workshop (WW5), vol. 1, pp. 193–206, 1981.

Sasaki, M., Yuge, A., Hayashi, T., Nishino, H., Uchida, M., and Noguchi, T.: Large capacity hydrostatic transmission with variable displacement, in: The 9th International Fluid Power Conference, vol. 9, 2014.

Schmitz, J., Diepeveen, N., Vatheuer, N., and Murrenhoff, H.: Dynamic transmission response of a hydrostatic transmission measured on a test bench, in: EWEA 2012, EWEA, 2012.

Schmitz, J., Vukovic, M., and Murrenhoff, H.: Hydrostatic transmission for wind turbines: An old concept, new dynamics, in: ASME/BATH 2013 Symposium on Fluid Power and Motion Control, pp. V001T01A029–V001T01A029, American Society of Mechanical Engineers, 2013.

Scipy.org: Interpolation (scipy.interpolate.RegularGridInterpolator), https://docs.scipy.org/doc/scipy-0.19.1/reference/interpolate.html, (last access: 2017-07-01), 2017.

Silva, P., Giuffrida, A., Fergnani, N., Macchi, E., Cantù, M., Suffredini, R., Schiavetti, M., and Gigliucci, G.: Performance prediction of a multi-MW wind turbine adopting an advanced hydrostatic transmission, Energy, 64, 450–461, 2014.

Skaare, B., Hörnsten, B., and Nielsen, F. G.: Energy considerations for wind turbines with hydraulic transmission systems, EWEA OFFSHORE, 2011.

Skaare, B., Hörnsten, B., and Nielsen, F. G.: Modeling, simulation and control of a wind turbine with a hydraulic transmission system, Wind Energy, 16, 1259–1276, 2013.

Spinato, F., Tavner, P., Van Bussel, G., and Koutoulakos, E.: Reliability of wind turbine subassemblies, IET Renewable Power Generation, 3, 387–401, 2009.

Thake, J.: The Micro-hydro Pelton Turbine Manual, Practical Action Publishing, Rugby, Warwickshire, United Kingdom, https://doi.org/10.3362/9781780445519, 2000.

Thomsen, K. E., Dahlhaug, O., Niss, M., and Haugset, S.: Technological advances in hydraulic drive trains for wind turbines, Energy Procedia, 24, 76–82, 2012.

Trostmann, E.: Water hydraulics control technology, CRC Press, 1995.

Van der Tempel, J.: Energy extraction system, has water pump attached to rotor, windmill for pumping water from sea, water system connected to water pump, for passing water pumped from sea, and generator connected to water system,, 2009.

White, F. M.: Fluid Mechanics, McGraw-Hill, New York, 7 edn., 2011.

Zhang, Z.: Flow interactions in Pelton turbines and the hydraulic efficiency of the turbine system, Proceedings of the Institution of Mechanical Engineers, Part A: Journal of Power and Energy, 221, 343–355, 2007.